CHALMERS
UNIVERSITY OF TECHNOLOGY

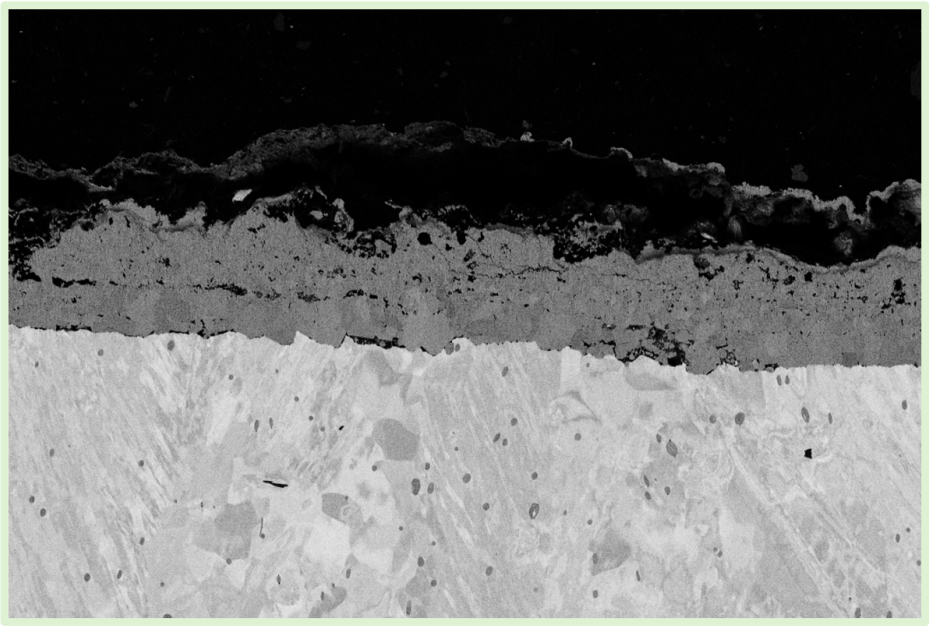

A microstructural investigation of Fe-oxides for developing high-temperature corrosion lifetime prediction models

Bachelor's thesis in Chemical Engineering

ALEXANDRA FLORA ALTO

Division of Energy and Materials, Department of Chemistry and Chemical Engineering

CHALMERS UNIVERSITY OF TECHNOLOGY
Gothenburg, Sweden 2026
www.chalmers.se

Chemical engineering Bachelor's Thesis 2026

A microstructural investigation of Fe-oxides for developing high-temperature corrosion lifetime prediction models

ALEXANDRA FLORA ALTO

CHALMERS
UNIVERSITY OF TECHNOLOGY

Division of Energy and Materials,
Department of Chemistry and Chemical Engineering
Chalmers University of Technology
Gothenburg, Sweden 2026

A microstructural investigation of Fe-oxides
for developing high-temperature corrosion lifetime prediction models
ALEXANDRA FLORA ALTO
Division of Energy and Materials,
Department of Chemistry and Chemical Engineering
Chalmers University of Technology

A microstructural investigation of Fe-oxides
for developing high-temperature corrosion lifetime prediction models
ALEXANDRA FLORA ALTO

Supervisor: Hampus Lindmark, Division of Energy and Materials, Department of Chemistry and Chemical Engineering
Examiner: Jesper Liske, Division of Energy and Materials, Department of Chemistry and Chemical Engineering

Chemical engineering project report 2026
Division of Energy and Materials, Department of Chemistry and Chemical Engineering
Chalmers University of Technology
SE-412 96 Gothenburg
Sweden
Telephone +46 723 660 888

Cover: figure from the SEM analysis of the Fe sample with KCl exposed to 20 % water vapor, 5 % O_2 and 75 % N_2 environment at 400°C for 168 h. The SEM is at magnification of 1000.

Typeset in LaTeX
Gothenburg, Sweden 2026

Abstract

The aim of this study was to investigate the microstructure of oxide scales formed in environments relevant to biomass- and waste boilers used for superheater applications. It also investigated how KCl can affect both the corrosion kinetics and microstructure, specifically the characteristics of oxide grain boundaries. The obtained data provides insights into high-temperature corrosion and ultimately help improve high-temperature corrosion lifetime prediction models for superheater tubes. The study starts with a literature review about corrosion and analytical methods. To simulate the environment that exists for the superheater tubes of biomass- and waste power plants, the furnace's environment was prepared to attain constant levels of the following: 20 % water vapor, 5 % O_2 and 75 % N_2 at 400 °C. Each exposure of the sample groups was performed according to four phases, namely sample preparation, exposure to simulation of the environment, preparation before SEM analysis, and SEM analysis.

Results showed that pure Fe samples exposed longer to the simulated environment experienced the corrosion process to a greater extent, which results in a thicker oxide scale on the Fe sample surface. In addition, KCl appears to have increased the corrosion rate, as demonstrated by the greater oxide scale thickness, the higher mass gain of the samples, and the observability of oxide grains after both exposure times. The combined use of SEM-EDS (EDX) made it possible to perform EDX mapping and EDX point analysis of the exposed samples. This facilitated the identification of the Fe sample surface, the Fe-rich oxide scales, and the KCl layer located on top of the oxide scales. The flat BIB milling technology implemented during sample preparation prior to SEM imaging enabled the identification and differentiation of oxide grains, BIB milling marks, and mechanical polishing scratches. This indicates that there is a need for improvement in the flat BIB milling technique, which could be achieved by testing variations in the accelerating voltage, the angle of incidence of the ion beam, and the flat BIB milling exposure time.

In conclusion, the flat BIB milling method, when combined with SEM, has the potential to reveal oxide grains at the nanoscale, making the observation of these oxide grains in the oxide scale more accessible than with widely utilized conventional technologies. Nevertheless, this study also shows that the method requires further development. Therefore, future work should focus on optimizing the BIB parameters to achieve the best possible Fe surface finish. Lastly, exposure time and the presence of KCl appears to have a positive effect on the detection of oxide grains and the growth of the oxide scale on pure Fe samples.

Keywords: SEM, flat BIB milling, oxide scale, corrosion, microstructure, oxide grain

Acknowledgements

First, I would like to thank Professor Jesper Liske for this opportunity to be a part of the High Temperature Corrosion (HTC) Centre at Chalmers University. Second, I also want to express my gratitude to Postdoc Hampus Lindmark for being a reliable academic advisor and for giving me the practical skills and background that were necessary to perform laboratory work and analysis both independently and with colleagues. Most importantly, I would like to thank my friends, family and classmates for being a united pillar of strength and support throughout my engineering journey.

During my time at HTC, I was able to learn about metallurgy and corrosion and how these can be utilized to further improve our energy sources to achieve a more sustainable community. I will bring both the engineering knowledge and experiences that I have gained with me in my further academic endeavours in chemistry, physics and beyond.

Alexandra Flora Alto, Gothenburg, March 2026

List of Acronyms

The following are acronyms that have been utilized in this chemical engineering bachelor thesis:

HTC	High Temperature Corrosion
CHP	Combined Heat and Power
GHG	Green House Gas
BIB	Broad Ion Beam
SEM	Scanning Electron Microscope
BSE	Backscatter Electron
EDS	Energy Dispersive Spectroscopy
EDX	Energy Dispersive X-ray

Contents

List of Figures

List of Tables

1
Introduction

Last year, the first group of the 11,000 Tuvalu residents in the South Pacific started their migration process to the Commonwealth of Australia [1, 2]. This is a move not driven by choice but is instead due to the danger brought by the rising waters around the island nation, and this can be considered to be an example of an immediate humanitarian consequence of the global warming caused by the increasing global carbon dioxide emissions [1]. The ongoing sinking of the Tuvalu islands underlines the inadequacy of the global search and result for the next alternative energy source that can hinder the consequences of the global warming [1, 3]. According to what has been agreed upon in the Paris Agreement, the rise of the global temperature is aimed to be below 2 °C [4]. Nevertheless, the increase in global temperature seems to be far from being either halted or slowed down [3]. This calls for an imperative solution that can bring about a significant decrease in carbon dioxide emissions.

When it comes to both electricity and heat production, there has been a heavy reliance on power plants that use fossil fuels namely coal, gas, and oil [3, 5]. It has been found that the central energy consumption from the usage of fossil fuels is 86 % [5]. Meanwhile, other energy sources only account for 14 % [5]. Although fossil fuels are major contributor to power production, it is worth noting that it has been projected that oil production has peaked in 2015, and gas and oil production will peak in the year 2035 and 2052 respectively [5]. It has been reported earlier that the number of oil reserves has been rising with the passing years due to new discoveries [5]. However, since oil is a finite natural resource, it will reach a point where there are no new oil reserves left to be discovered [5]. Thus, it is approximately expected for oil reserves to be depleted in the year 2066 [5]. This highlights that fossil fuels taken from natural reserves will be depleted with time and that it is important for the energy industry to be able to find alternative energy sources that can also be sustainable for the environment [5].

The current continuous exponential increase of global population is a factor that is affecting energy production today and the coming future [5, 6]. This corroborates the importance of the understanding that the current energy production is based on finite fossil fuel reserves [6]. With the increasing population, comes the increase in demand for heat, fuel and energy as well as consumer goods [6]. To sustain the exponential increase of population requires an alternative solution to energy production to ensure that the future generation will not solely be reliant on the depleting fossil fuel resources to produce heat, energy and products of necessity [6]. Consequently, it is important for the current generation to find energy alternatives that both will

make the current fossil fuel power plants more efficient and find alternative sustainable energy sources [5].

Both the goal to decrease the carbon dioxide emission and finding alternative ways to be less dependent on fossil fuels have led to European countries to utilize waste and biomass as fuel alternatives [7, 8]. A power plant that produces both heat and electricity which is also known as combined heat and power (CHP) plants have been implemented in many European countries [7]. CHP takes advantage of the huge waste that is placed in the landfill and turning it into fuel for power production [7]. However, CHP plants have had challenges with the burning of waste and biomass as the combustion process produces corrosive products which ultimately damage parts of the boiler decreasing both efficiency and power plant lifetime [3, 9]. This shows that studies focusing on investigating which materials are suitable for boilers to be able to adapt to corrosive environments are needed to increase waste and biomass power plants relevance against fossil fuel power plants [3].

At the global stage, there are two countries that lead the use of power plants that use waste and biomass as fuel for power production per capita namely Finland and Denmark as illustrated by the figure below [8].

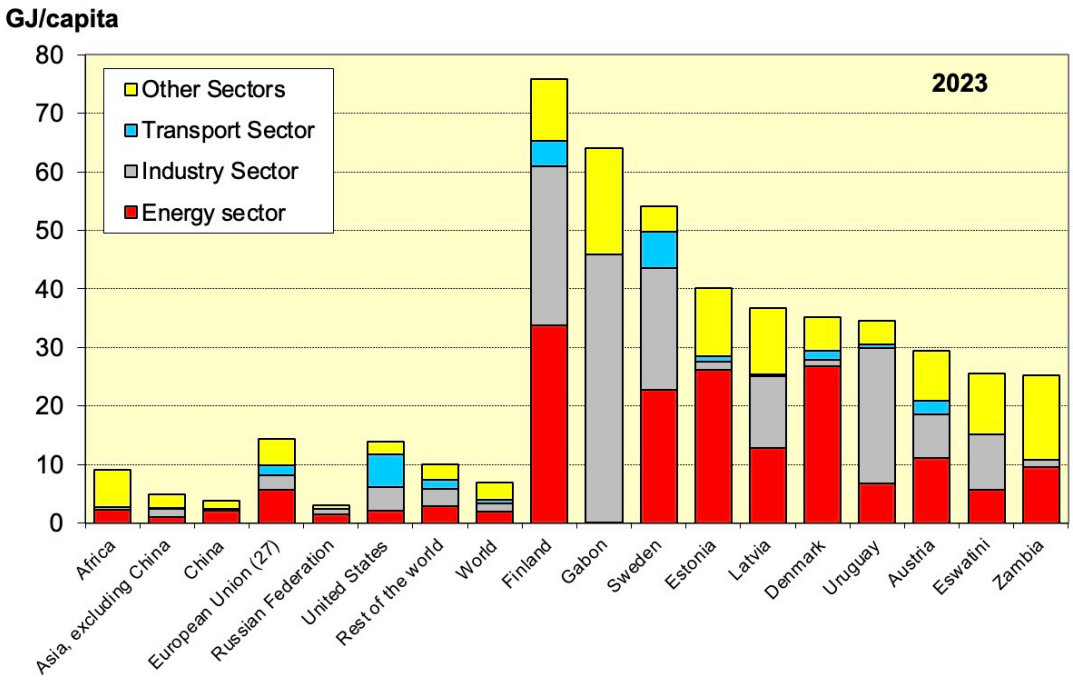

Figure 1.1: shows an illustrative comparison of various countries and global regions that use biomass and waste for power production per capita. This figure is adapted from the following source material [8].

Moreover, the heat produced from the usage of biomass fuel and waste fuel make up around two-thirds of the district heating in Sweden [8]. A reliance on biomass fuel may also cause a problem for the next generation since this can give way to the inception of increase in biomass resource competition in Sweden [8]. This may result

to both price increase of biomass resources and total price of heat and electricity for communities and households [8].

As Sweden has embarked on achieving an ambitious environmental milestone, it aims as a country to have attained a net-zero emission of greenhouse gas in the year 2045 [10]. This calls for finding solutions on how to accurately predict lifetime models of power plants in order to increase and strengthen both competitiveness and global positioning of biomass and waste power plants as a sustainable energy source [3, 8]. As a result, the inevitability of conducting a material investigation of biomass and waste power plant boiler namely superheater tube parts arises [3].

1.1 Background

It has been reported that around 60 % of the total global carbon dioxide emission comes from the production of both heat and electricity [11]. Power production has been reliant for a prolonged period on fossil fuel, which has contributed to the increase of atmospheric carbon dioxide levels [3]. This highlights the importance of developing more sustainable power plants such as biomass- and waste power plants to generate power [3]. However, combustion of biomass fuel or waste fuel in the boiler and its smaller parts superheater tubes can cause the formation of corrosive substances, namely KCl and HCl among many [3, 12]. Below is an image that shows a waste power plant with superheater tubes in it [3].

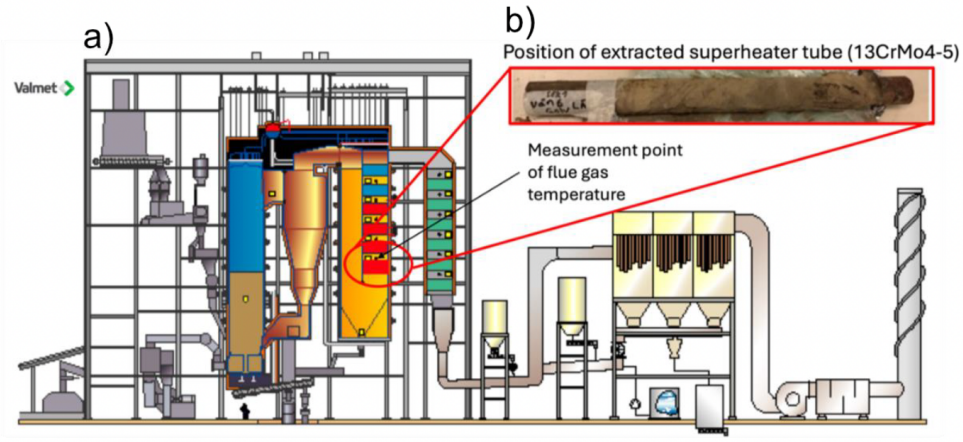

Figure 1.2: the figure shows in a) a waste power plant and in b) a superheater tube, and this figure is adapted from the following literature [3].

With the mixture of corrosive substance and exhaust gas from the combustion in the boiler, the rate of the corrosion process of the superheater tube material increases [3]. For this to be prevented, the steam temperature of the boiler can be decreased or another material that has more corrosion resistant property can be utilized [3]. Furthermore, decreasing the steam temperature causes the reduction of the enthalpy of the steam that goes into the turbines and as a result the efficiency of the

power plants reaches a lower range of 18 % and 37 % [3, 13]. This presents a problem since the efficiency of biomass- and waste power plants must be increased for it to be seen as a significant alternative to fossil fuel power plants in the global stage.

Superheater tubes are commonly made of alloys and two examples are FeCr and FeCrNi [12]. During high-temperature corrosion, they initially form a protective scale and once this protection loses its strength, a secondary Fe-rich oxide scale formation takes place [3, 12]. This Fe-rich oxide scale does not provide a sufficient corrosion resistance which leads to the further corrosion of superheater tubes [3]. The formed oxide scale also comes with defects and one example of this is the oxide grain boundary, which is an important factor in the corrosion rate at high-temperatures ranging between 400 °C and 600 °C [3]. Since the rate of diffusion of ions through the oxide grain boundary increases at high temperature, it raises the importance of understanding the microstructure of the Fe-oxides with both new analytical techniques and technologies [3]. A broader understanding of Fe-oxide microstructure may provide new data that can be used to form a more accurate lifetime predictive models for superheater tubes.

1.2 Purpose

This work aims to further develop and evaluate the microstructural methodology of previously performed research within biomass- and waste fired boiler [3]. Laboratory investigations in an environment that can simulate the corrosive environment within superheater tubes that are located in the boiler of a biomass- and waste fired power plant [3]. To model the superheater structure and its response to corrosive environment, pure Fe sample is utilized due to its ability to form Fe-rich oxide scale which has corrosive and protective characteristics that can be argued similar to the Fe-rich oxide scales that can be formed on stainless steel surfaces after going through breakaway corrosion [3]. Furthermore, the usage of pure Fe gave way to the ability to investigate whether KCl has any effect on the growth or development of oxide microstructure specifically oxide grain boundaries in corrosive environments [3]. The data that will be generated can be characterized as both new and unique, and it may even be utilized as a ground to improve high-temperature corrosion lifetime prediction models for superheater tubes [3].

1.3 Limitations

Due to the time constraint and the limited number of trials that can be performed, this thesis can be seen as an early investigation and the results can be considered as a starting ground for high-temperature oxide grain database. Superheater tubes of biomass and waste power plants today are constructed with Fe-based alloys and not pure Fe analyzed in this study [3]. This suggests that there should be a careful generalization of the presented results.

2

Theory

To understand high-temperature corrosion on pure Fe, it is important to be acquainted with how thermodynamic factors such as kinetics, crystal defects, grain boundary, and length of exposure to environment can play a role in the extent of corrosion that a pure Fe structure can undergo [3, 14]. It is also important to know which analytical methods can be used to analyze the extent of corrosion on pure Fe samples exposed to a certain environment and temperature [3]. The following will then describe concepts within high-temperature corrosion and analytical methods to analyze the rate of corrosion and the observation of the oxide grain.

2.1 Oxide and thermodynamics

When exposed to corrosive environments, metals such as pure Fe prefer to be in their less energy requiring oxide form [15]. Fe oxides are also considered to be more thermodynamically stable [15]. Whereas, the pure Fe requires a higher amount of energy to stay in its form [15]. To be able to quantify this, it is important to look into the values of Gibbs free energy whose relationship with enthalpy change, entropy change and temperature is shown by the following:

$$\Delta G = \Delta H - T\Delta S \tag{2.1}$$

where a value of ΔG less than zero implies the spontaneity of the chemical reaction where the pure Fe will be oxidized [3].

To have a closer understanding of Fe oxides' thermodynamic stability, it is important to consider both dissociation pressure of oxygen (p_{O_2}) and values of standard Gibbs free energy (ΔG°) [3]. At a given temperature, the oxide with the lower equilibrium oxygen partial pressure is the more thermodynamically stable oxide. Consequently, a lower p_{O_2} corresponds to a more negative tendency for oxide formation and greater oxide stability [3]. In addition, the relationship between p_{O_2} and ΔG° of metal oxides can be derived as shown by the following:

$$\Delta G^\circ = RTln(p_{O_2}^{\frac{y}{2}}) \tag{2.2}$$

if equilibrium around the metal is established ($\Delta G = 0$) [3].

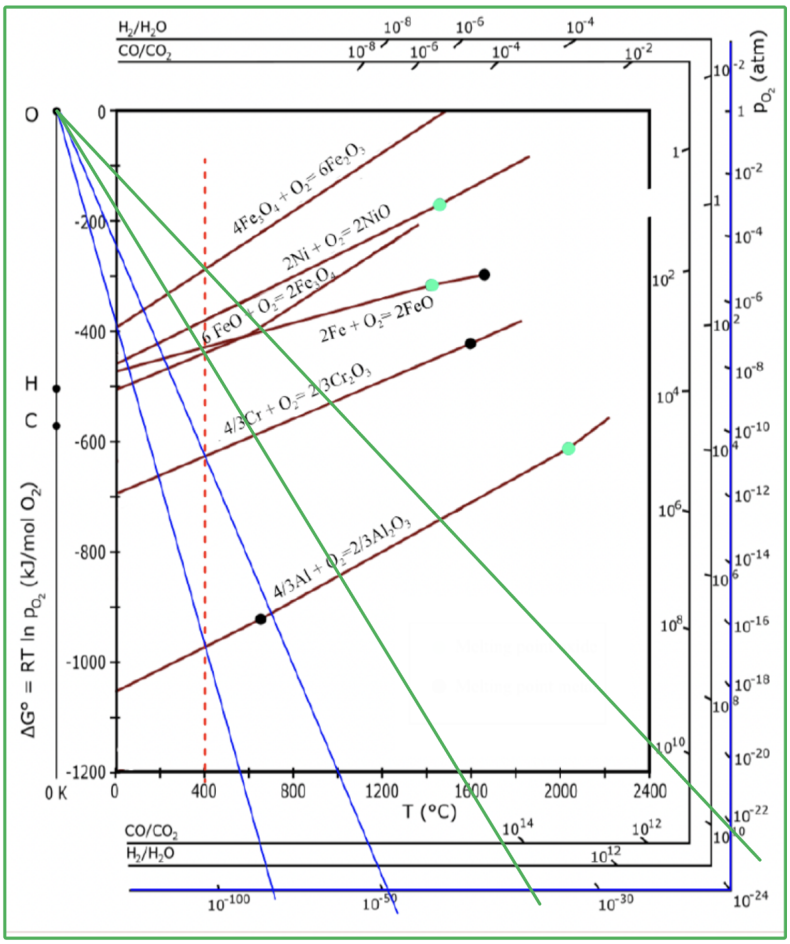

Figure 2.1: presents a figure of the Ellingham-Richardson diagram which shows the corresponding dissociation pressure of oxygen (p_{O_2}). This figure is adapted from the following source material [3].

With the help of the temperature 400 °C and by following the green lines that starts from O in figure (2.1), the individual (p_{O_2}) values for magnetite (Fe_3O_4) and hematite (Fe_2O_3) are 10^{-37} atm and 10^{-22} atm respectively. Consequently, the magnetite oxide scales will be expected to firstly form on the surface of the Fe sample [15].

2.2 High-temperature corrosion

In metallurgy, corrosion can be described as the deformation of the metal structure that is caused by chemical reactions that are in the nearby environment [14]. Rusting is a common example of corrosion and this process takes place due to a metal's interaction with oxygen and water molecules in its surrounding environment [14].

One example of this is when pure Fe loses its electrons and as a result producing Fe ions that then forms oxides with the surrounding oxygen namely Fe_3O_4 and Fe_2O_3 which are called magnetite and hematite respectively [15]. Both magnetite (Fe_3O_4) and hematite (Fe_2O_3) oxides form on the surface of Fe material when it is exposed to high-temperature corrosive environment where the temperature range is less than or equal to 570 °C [15].

2.2.1 Oxide grain and oxide scale at high temperature

When an oxide scale is formed due to corrosion of a metal surface at high temperature, an oxide grain can be observed depending on the present molecules and the temperature of the surrounding environment [15]. Moreover, the type of metal or alloy that is exposed to corrosive environment can also affect both the size and number of oxide that can be found in the oxide scale [3]. Previous studies have shown that Fe exposure to environment of 40 % water vapour at 400 °C for 24 h leads to corrosion where the oxide scale thickness can reach up to 1.9 μm [15]. In addition, it was also found that oxide grain can be observed in the central part of the oxide scale as shown in the figure below [15].

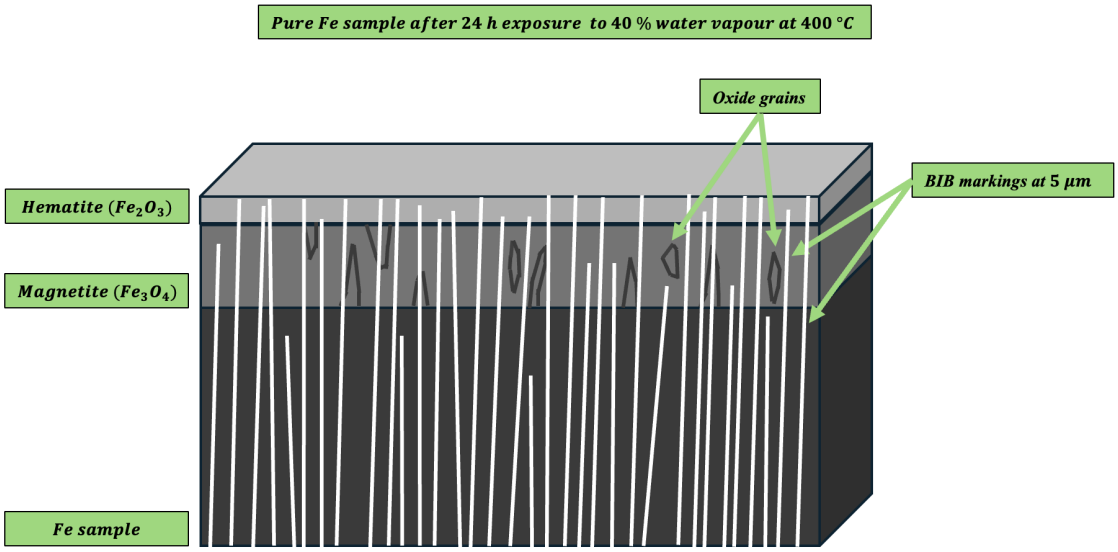

Figure 2.2: shows a simplified microstructure illustration of pure Fe sample exposed for 24 hours in a furnace with an environment of 40 % water vapor at 400 °C, and the figure created is based on the results of the following literature [15].

2.2.2 Ion diffusion at high temperature

Ion diffusion through an oxide scale layer can take place through either the lattice (bulk) structures or grain boundaries as described by the figure below [3, 16].

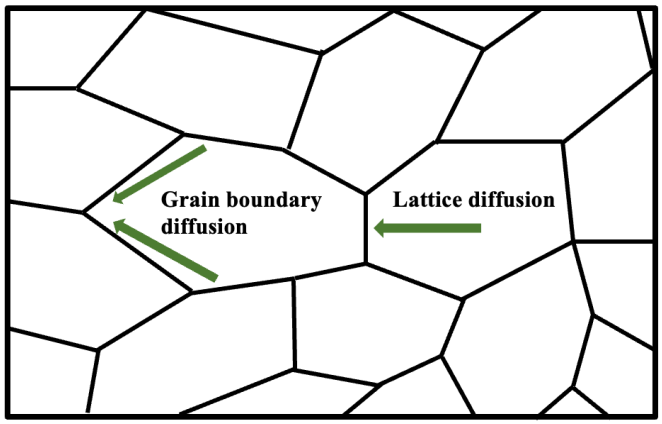

Figure 2.3: the figure shows a simplified representation of the grain boundary diffusion and lattice diffusion, and this illustration is based on the description of the following literature [3, 16].

In the lattice structure, defects can be present and these defects are due to vacancy or the existence of interstitial areas [3]. Vacancy defect in the lattice structure allows ions in its original position to move towards a vacant space while the presence of an interstitial area allows for example an ion to diffuse to another area that tangents the ion's original position [3].

Previous high-temperature (750 °C to 900 °C) study on Fe-based FeCr alloy have shown that the grain boundary diffusion coefficient (D_{gb}) of ions appears to be higher than the lattice diffusion coefficient (D_l) [17]. This result was also found to be true for the drift temperature (400 °C to 600 °C) of superheaters [3]. It was also previously reported that both values of D_{gb} and D_l contribute to the total diffusion of ions in the oxide structure, which allowed the derivation of the effective diffusion coefficient (D_{eff}) expression below [3].

$$D_{eff} = D_l(1 - f) + D_{gb}f \tag{2.3}$$

The value for f can be obtained from dividing the oxide grain's width by the size of the oxide grain [3]. As the definition of D_{eff} implies, the higher the number of oxide grains there is in an oxide scale layer, the higher the value of D_{gb} and D_{eff} will become [3]. Both the temperature and the quantification of the oxide grain size appear to be essential for understanding diffusion rates of ions in the oxide scale layer and how this can influence corrosion rate [3, 17].

2.2.3 Oxide growth at high temperature

As a metal sample is exposed to a corrosive environment for a certain period of time, the oxide scale formation will start to occur, and this process can be fundamentally described with a three-step mechanism as shown below [3].

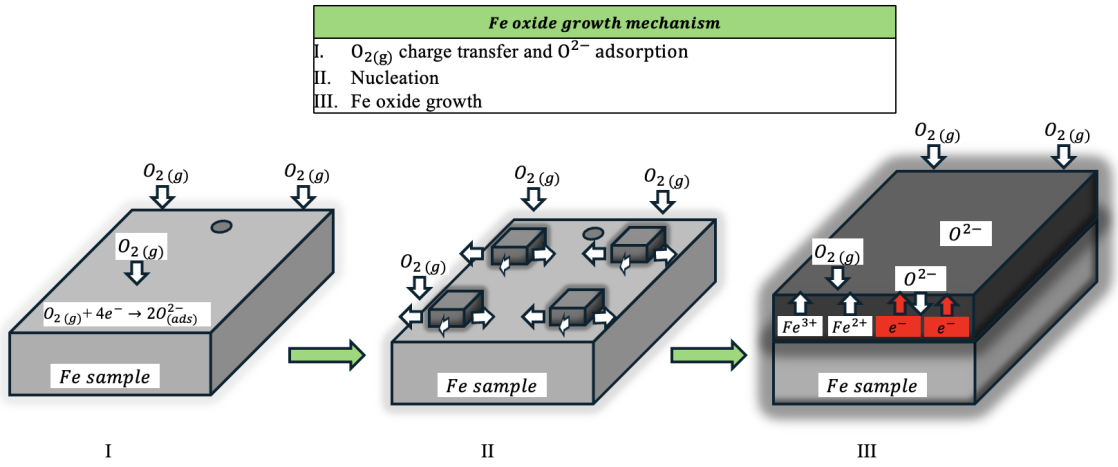

Figure 2.4: presents a simplified illustration of the three-step Fe oxide growth, and this was based on the description of the following literature [3].

In high-temperature corrosive environment, the first and second steps in figure (2.4) will take place at a higher rate than in corrosive environment of lower temperature [3]. In the first step, $O_{2(g)}$ reacts with the metal on the surface and forms an oxides which then becomes nuclei of oxides [3]. These oxide nuclei then settles on the metal surface and with time these grow on the surface creating a homogeneous layer [3]. The oxide scale will then continuously grow where the metal ions and electrons diffuse along the oxide layer [3]. At a certain time, the oxide scale will be compact and thicker enough to have a decreasing effect on the oxidation rate since these can hinder the diffusion of metal ions along the thicker and more compact oxide scale [3]. The overall oxide growth mechanism is based upon parabolic kinetics [3].

2.2.4 Breakaway corrosion at high temperature

Superheaters that are made of Fe-based alloys such as FeCr and FeCrNi can initially form a first protective oxide scale when exposed to both high-temperature and corrosive materials [3]. High-temperature ranges between 400 °C and 600 °C while examples corrosive products are KCl, HCl and water vapor [3]. Prolonged exposure to this environment causes the formation of the oxide scale that is made up of Fe oxides [3]. Consequently, this can be called the second layer of oxide scale protection of Fe-based alloy material [3]. This phenomenon is widely called breakaway corrosion within metallurgy and an illustration of this from previous literature can be observed below [3, 18].

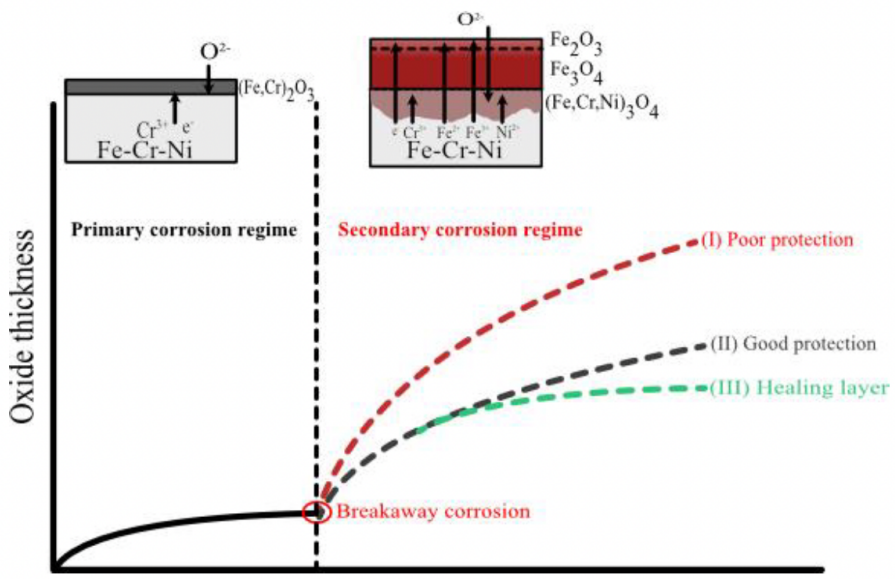

Figure 2.5: the figure shows oxide thickness against time in FeCrNi corrosion. The figure is adapted from the literature [3].

Previous experiments also found that the presence of KCl and water vapor in the surrounding environment of alloys such as FeCrMo at 400 °C can cause the oxide scale to be more susceptible to forming cracks which also appears to increase the probability of the oxide scale to detach from the alloy surface [3, 18]. As a result, corrosion occurs again on the same surface of the alloy [18].

2.3 Corrosion and kinetics

Corrosion kinetics at temperatures that are higher than or equal to 400 °C can be described using different kinetic models [15]. Oxidation growth behaviors are linear, parabolic, and logarithmic whose respective behavior is illustrated below [15].

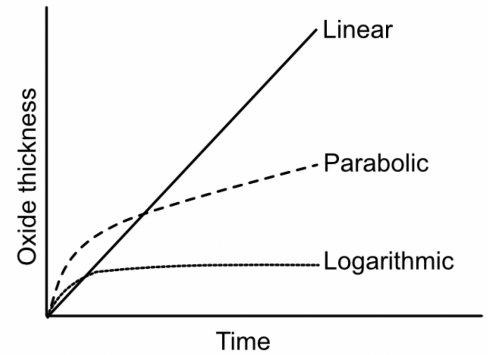

Figure 2.6: presents an illustration of the relationship between time and oxide thickness. This figure is adapted from the following literature [3].

If an oxide growth follows a linear rate law, this generally indicates that the oxide scale is repeatedly detached from the metal surface, exposing fresh metal surface to

the environment and thus reinitiating the corrosion process [3]. Parabolic oxidation kinetics may indicate that the oxide scale is protective and remains adherent to the metal surface [3]. As the oxide scale gains thickness with time, the diffusion of ions such as Fe ions and oxygen ions through the scale becomes slower as the oxide scale grows, which slows down the oxidation rate over time [3]. In this case, corrosion process continues, but at a decreasing rate [3]. Typically, the rate determining step is the diffusion of ions through the oxide scale and thus the microstructure of the oxide scale such as oxide phase and oxide grain size plays an important role [3]. The parabolic oxide growth that is typical at high temperature for alloys is important for superheaters, and this can be expressed with the following relationship:

$$X^2 = K_p t + C \tag{2.4}$$

where X equals either mass gain or oxide thickness, Kp is the rate determining constant, t is time, and C is an integer [3]. If oxide growth follows a logarithmic rate law, this could indicate the formation of a very thin and highly protective oxide scale, where oxidation is initially rapid but slows down significantly as the scale thickens [3].

2.4 Analytical techniques and technologies

The rate of corrosion of pure Fe and its subsequent microstructure can be investigated with the help of scanning electron microscope (SEM) and broad ion beam (BIB) milling [3]. This section aims to describe these technologies and how they can be used to analyze Fe samples to gain information about its microstructure.

2.4.1 BIB milling

Mechanical polishing of pure metal or alloy samples are commonly used to prepare samples that are going to be analyzed with SEM [3, 19]. It is also possible to analyze samples at a higher precision with SEM by performing BIB milling on the sample's uneven surface, and the following figure demonstrates the difference between a sample surface that is polished mechanically and a sample surface that is both mechanically polished and run with BIB milling [3].

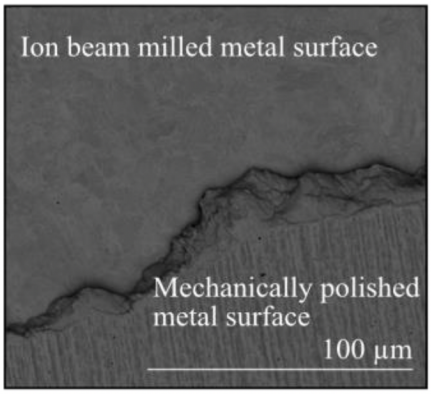

Figure 2.7: the figure shows a comparison between a sample surface that is solely polished mechanically and a sample surface that is both mechanically polished and run with BIB milling. The figure is adapted from [3].

With BIB milling, the sample is placed in a chamber of the BIB instrument that maintains a vacuum environment [3]. Electrical voltage is then used to move the argon ions towards a cathode, and this forms an ion beam which aims directly to the sample's surface as described by the following figure [3, 19].

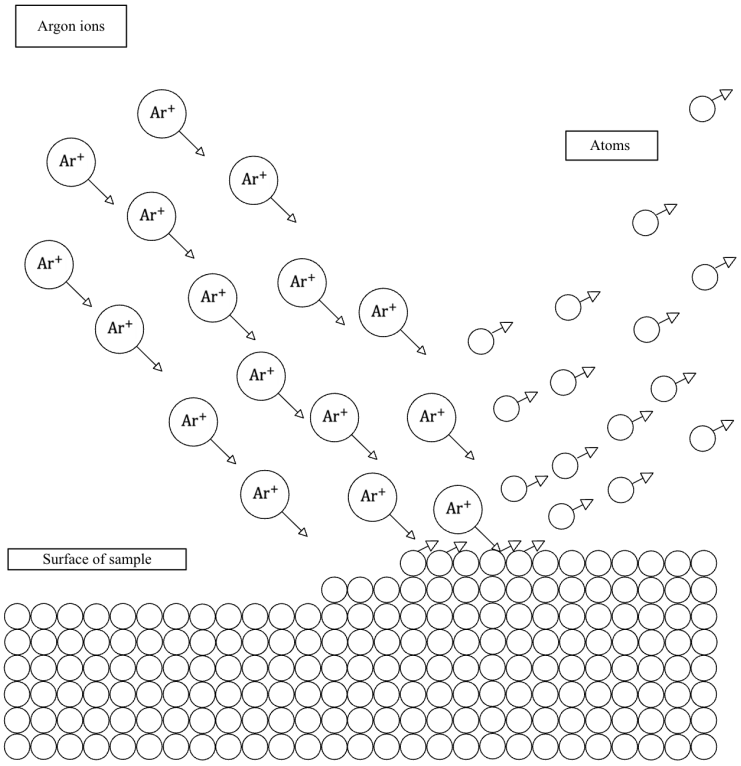

Figure 2.8: the figure shows an overall presentation BIB milling where argon ions with high energy are aimed towards the sample's surface, and this figure is based on the descriptions of the following literature [3, 19].

The ion beam allows for the controlled breakage of atomic bonds on the sample's

surface, and this makes it possible for the sample to have a surface that can be analyzed at a nanolevel [3]. One factor that also affects the finish of the sample's surface is the angle of the beam of argon that is pointing towards the surface of the sample [19]. A lower angle allows to attain a more polished surface while a higher angle allows the exposure of the surface sample's microstructure characteristics [19]. There are two types of BIB milling namely flat milling and cross-sectional milling [3, 19]. Flat BIB milling allows for the alteration of the argon ions' angle between 0° and 90°, which is a range that makes it possible for the ion beam to be almost adjacent to the center of the center of the sample [3]. This is the method that is commonly used when investigating a sample's microstructure [3].

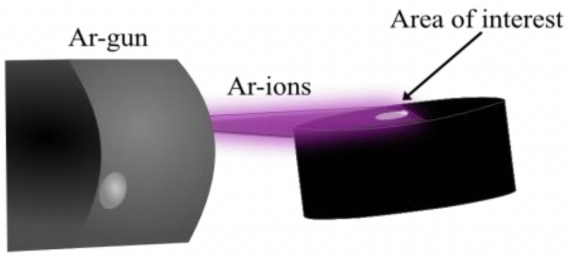

Figure 2.9: the figure illustrates how flat BIB milling is implemented on the surface of the sample. The figure is adapted from [3].

2.4.2 SEM and EDS (EDX) technology

SEM has a number of area applications such as in life science and microscience since it allows researchers to study areas that can be as small as 10 μm [20]. At this level of precision, SEM enables the microstructural analysis of the samples [3]. SEM then becomes a tool that can be used to analyze the surface of the samples to understand the effect of high-temperature corrosion [3, 20]. This microscope takes advantage of the magnetic fields that come from the electrons, and these electrons are emitted by the gun in the SEM [20]. Furthermore, the emitted electrons pass through an electrical field, which works as a tool to maneuver the direction of the electrons towards the surface of the sample [20].

A combination of energy dispersive spectroscopy (EDS) detector and SEM can be utilized for microanalysis [3, 21]. EDS can be even called energy dispersive X-ray (EDX) analysis in other context [22]. This SEM-EDS combination is a way for a sample to be analyzed, and the figures that will be gathered are of high spatiality resolution [12]. These figures may also provide a characterization of which elements a sample may have in specific regions [3]. For SEM-EDX coupling to be able to produce figures, the incident electron has to emit enough energy between the atoms in the sample and the incident electrons as described in the figure below [3].

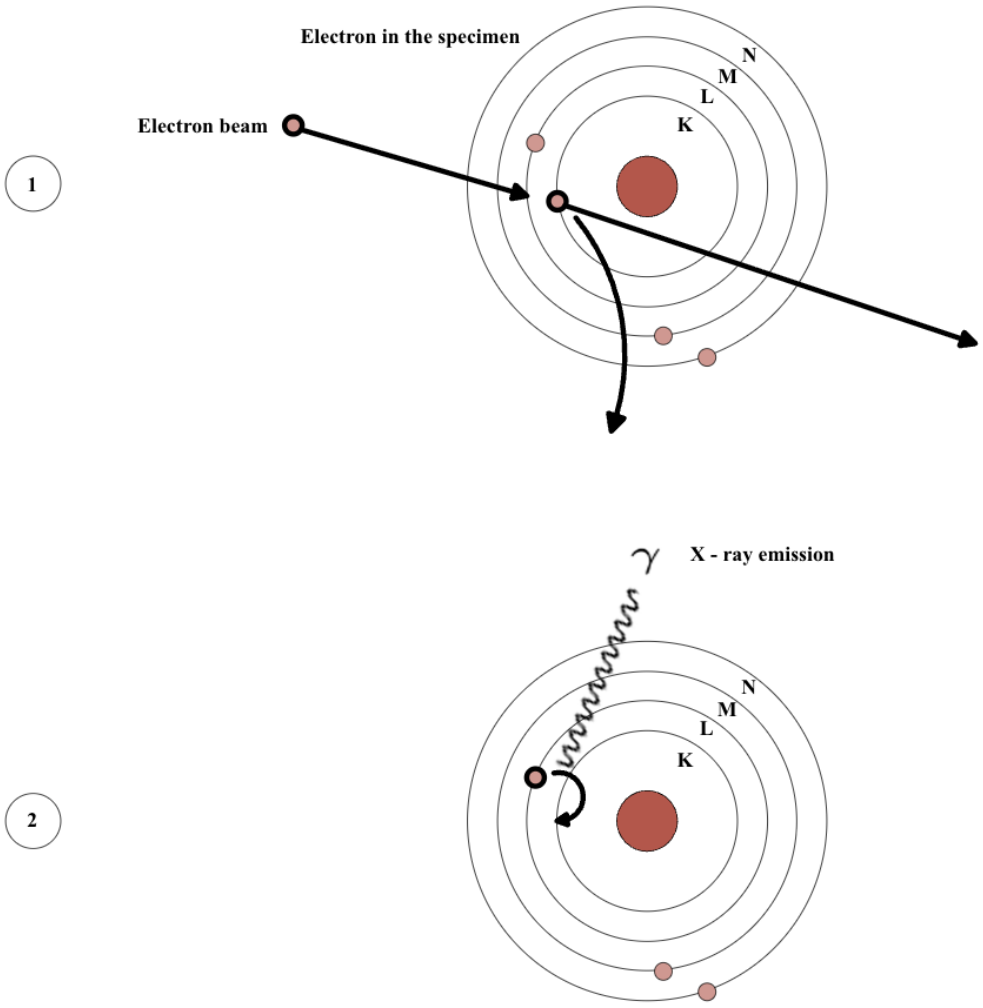

Figure 2.10: shows a simplified illustrative figure of an electron beam colliding to another electron in an atom, and this is based on the descriptions of the following literature [3].

The primary electrons from the SEM-EDS tandem hit the sample surface as an electron beam, which causes the removal of the surface atom's electron [3]. This causes an energy instability within the atom, and to solve this an electron from a higher energy level takes the place of the removed electron [3]. As a result, this transfer of electrons from a higher level to a lower unoccupied lower level releases electromagnetic radiation in the form of X-ray, and this is what SEM-EDS coupling detects [3].

2.4.3 SEM and BSE technology

SEM can also be paired with a backscattered electron (BSE) detector [3, 18]. As illustrated by the figure below, this combination works by using a scattered electron

in an elastic manner, and this electron then hits the sample which then leaves the sample as a backscattered electron [18].

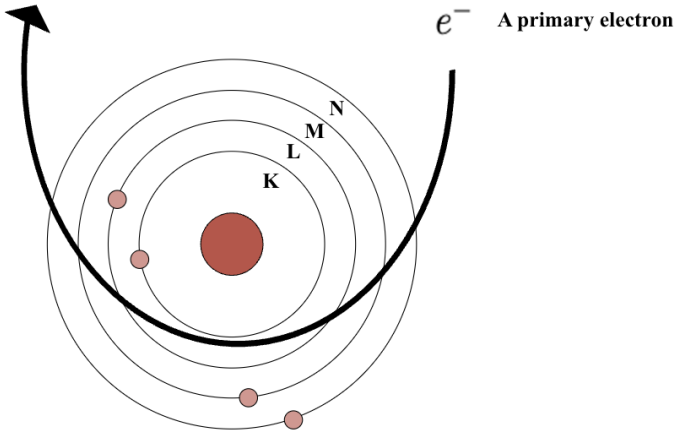

Figure 2.11: shows a simplified figure illustrating a primary electron that goes around a nucleus of an atom in a sample, and this is based upon description in the following references [3, 18].

Moreover, there is a proportionality in the relationship between the number of backscattered electrons that pass through the metal sample and the atomic number of the sample [18]. This implies that if an area in a sample has a higher number of atomic number there are more backscattered electrons that will leave the sample, and these backscattered electrons will then be detected [18]. Hence, this specific area will appear brighter in the SEM-BSE figures that will be produced, and the converse is true for an area of the sample with lower atomic number [18]. For this reason, the SEM-BSE tandem allows for the identification of regions along the metal sample and the oxide scale [3, 18]. In addition, this can also be used to identify the thickness of the oxide scale on the surface of the metal sample after exposure [18].

3
Methods

The study starts with a literature review focusing on the theoretical background within corrosion, thermodynamics, microstructures, and analytical methods. In order to simulate the environment that exists within the superheater tubes, the furnace's environment was altered to attain constant levels of the following: 20 % water vapor, 5 % O_2 and 75 % N_2 at 400 °C. For these parameters to be achieved, the total air flow of 1000 ml/min in the furnace consisted of 238 ml/min of O_2 and 762 ml/min of N_2. To uphold a 20% water vapor in the air flow, a water bath with temperature of 60.4 °C was used. The furnace has a setup which is described in the figure below.

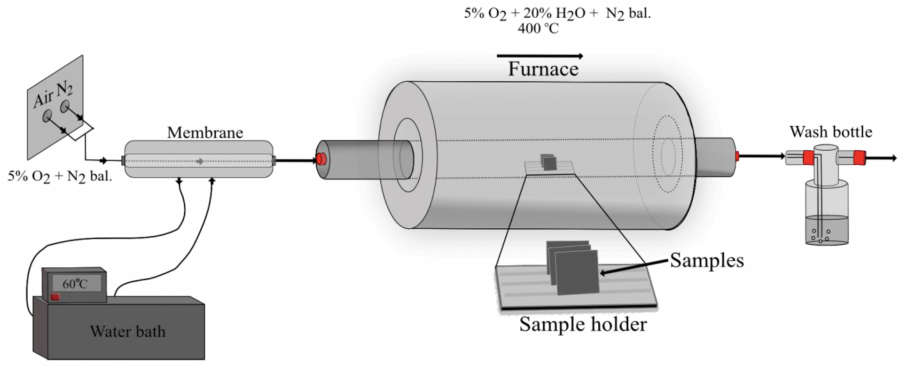

Figure 3.1: shows a figure of the furnace setup and other laboratory equipment that were connected; namely, water bath, wash bottle and membrane. The figure is from the the following literature [3].

Each exposure of sample groups was performed according to four phases namely sample preparation, exposure, preparation before SEM analysis, and SEM analysis.

3.1 Sample preparation

To prepare the pure Fe samples, the dimensions, area and weight of each pure Fe sample were determined in order to perform gravimetric analysis. The pure Fe samples that were utilized had an individual area between 3.38 cm^2 and 3.77 cm^2, and height of 14.5 mm as well as a length of 9.50 mm. In addition, the Fe samples also had a drilled hole on top of them to ease the samples' KCl coating, and the length of the hole was around 1.90 mm. This was taken into consideration when calculating the samples' area. The Fe samples were then polished on all sides to

achieve a mirror-like appearance, and this was performed by mechanically polishing the samples with silicon paper (SIC) that had a grit size 380 to 4000 and with the help of water as lubricant. The samples were then placed in plastic-labeled containers. In order to achieve a more mirror-like finish on both sides of the samples, a mechanical polishing with diamond suspensions were utilized that has a size of 9 μm, 3 μm and 1 μm. This was performed with oil as a lubricant. Acetone was used to clean the samples, and the samples were also submerged in acetone in their respective centrifuge tube. Thereafter, the samples in their centrifuge tubes were submerged in an Elmasonic P ultrasonic bath for 15 min.

3.2 Coating of samples with KCl

The first group of samples were simply exposed to the furnace for either 24 h or 168 h without KCl coating. The second group of Fe samples were coated with KCl before being exposed in the furnace for 24 h and 168 h. To coat the samples, they were manually sprayed with a solution that contains KCl, 80 % ethanol and 20 % water. The spraying was performed until the surface of the sample has 2 mg/cm^2 of KCl on it, and this was ensured by weighing the samples.

3.3 Fe and Au sample exposure

The exposure of the pure Fe samples was either run for 24 h or 168 h. There were even two groups of Fe samples where the first group consisted of the pure Fe samples. The second group was sprayed with KCl on both sides where it was aimed that the samples had to attain an almost identical amount of KCl on their surfaces. This was performed to investigate if the KCl which can be found in a biomass- and waste power plant's boiler has an enhancing effect on the corrosion rate of the pure Fe samples. Since samples with KCl on their surface will be exposed inside the furnace with constant airflow, it was important that KCl did not sublime so that the Fe samples' surface will have a uniform amount of KCl throughout the exposure time. The attempt to prevent sublimation of KCl from the Fe samples was carried out by placing a crucible with 53.58 g of KCl in the furnace. This crucible was then placed first in the furnace and the sample holder with the Fe samples on top was placed second.

The prevention of KCl sublimation was even tested by running furnace exposure with gold (Au) samples, which were sprayed with KCl on their surfaces to attain a constant amount of KCl on their surface. The exposure of the gold samples lasted for one hour, and a gravimetric analysis of the gold samples was performed to see if the mass of the gold samples with constant amount of KCl will have the same mass after an hour of exposure in the furnace. The use of gold was based on its physical property, and therefore was expected not to experience corrosion in the given furnace environment. Before the sample exposure was performed, the furnace was calibrated to ensure that the samples on their alumina holder will be at a tem-

perature as close to 400 °C. The crucible containing KCl was placed in the furnace where the temperature had a drop of around 1.0 °C or more, and this position was above the placement of the samples.

3.4 Sample preparation for SEM

The samples after exposure in the furnace were prepared for SEM cross-sectional analysis through gold sputter coating, sample cutting, bakelite mounting, polishing, and BIB milling. Once the samples had been covered with gold, they were cut into two smaller pieces for bakelit mounting. The cut part with a hole was used, and it had to be made sure that it was in a standing position during the bakelit preparation because this will make cross-sectional analysis possible. The prepared sample was also mechanically polished but without water as a lubricant, and the diamond polishing was also performed to achieve a mirror-like surface. The result of these processes is shown below.

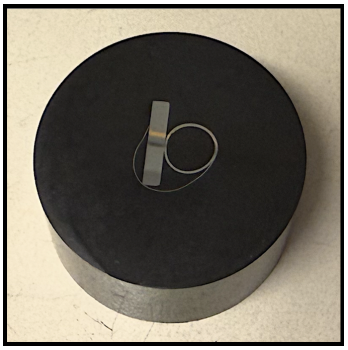

Figure 3.2: shows a figure of the exposed Fe sample after the preparation for SEM imaging.

Flat BIB flat milling was then performed with an accelerated voltage of 5 kV and an incident angle of Ar ion beam of 5°. This was also carried out for 15 min. Thereafter, gold sputter coating was performed on the sample.

3.5 SEM sample analysis

For SEM analysis, the figures of the prepared post exposure samples were taken with 5 kV - 6 kV setting while for the SEM-EDS combination a setting of 20 kV was implemented. Magnification can be found in appendix A.

3.6 Usage of program

Figure 2.2, figure 2.3, figure 2.4, figure 2.8, figure 2.10, and figure 2.11 were created with the help of Visio, ChemDraw and PowerPoint programs. For the presentation

of the SEM figures of samples, the PowerPoint application on MacBook Pro was utilized.

4

Results

Below are the gathered analysis and figures from the use of SEM and from the gravimetric analysis for the various environment and time exposure of the pure Fe samples to simulate the environment of the superheaters in the boiler. The furnace where the Fe samples were placed was given an environment where the air flow has 20 % water vapor, 5 % O_2 and 75 % N_2 at 400 °C at either 24 h or 168 h of exposure. In appendix A, the raw data from SEM analysis can be found.

4.1 Results from Fe samples' gravimetric analysis

In this section, the gravimetric results are presented in the following tables and figures. Table 4.1 and figure 4.1 present the gravimetric results for pure Fe and pure Fe with KCl that were exposed in the simulated superheater tube environment at the furnace at various exposure times at 400 °C.

Table 4.1: shows the mean mass gain of the pure Fe samples according to the exposure times. The Fe samples were exposed to 20 % water vapor, 5 % O_2 and 75 % N_2 at 400 °C.

Exposure time (h)	**Fe mass gain (mg/cm^2)**	**Fe & KCl mass gain (mg/cm^2)**
24	0.6755	1.3299
168	1.3652	4.4332

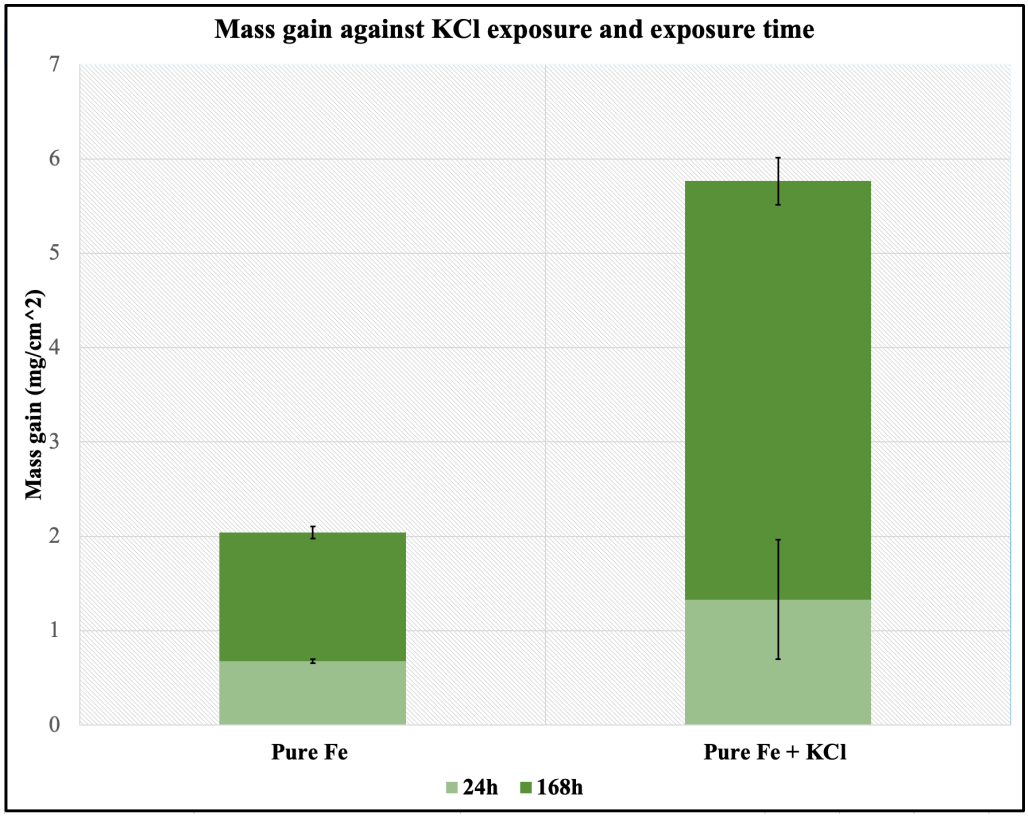

Figure 4.1: oxidation kinetics through mass gain of pure Fe sample and pure Fe with KCl samples in 20 % water vapor, 5 % O_2 and 75 % N_2 at 400 °C.

4.2 Results from Au samples' gravimetric analysis

For Au samples, the mass of alumina crucible containing KCl is 53.5838 g before exposure. After an hour of exposure, its mass was found to be 53.3285 g.

Table 4.2: shows the mass of Au with KCl samples before and after one hour of exposure to 20 % water vapor, 5 % O_2 and 75 % N_2 at 400 °C.

	Au & KCl mass(g)
Before 1h exposure	1.0758
After 1h exposure	1.0753

4.3 Imaging results from SEM-EDS (EDX)

The figures from SEM-EDS below show the result of the simulated environment of the superheater tubes. These allowed EDX mapping and EDX point analysis. The raw version of the figures can be found in appendix A.

4.3.1 Pure Fe sample exposed to the environment simulation for 168 h.

The following figures show the results of the pure Fe sample exposure to 20 % water vapor, 5 % O_2 and 75 % N_2 environment at 400 °C for 168 h.

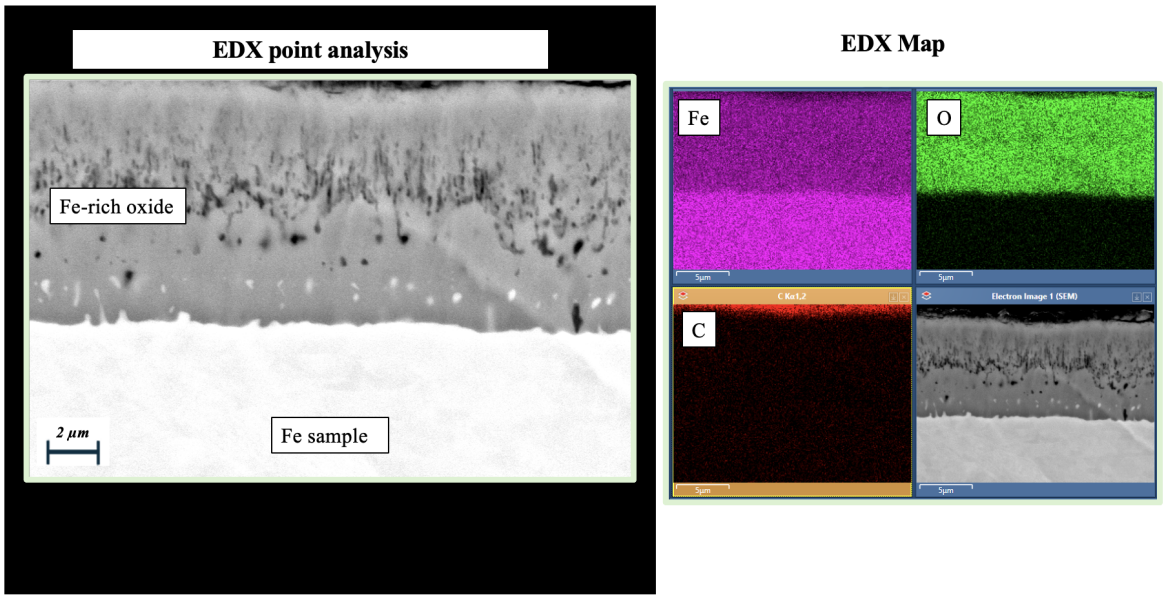

Figure 4.2: shows the SEM-EDX figure of Fe sample exposed for 168 h.

4.3.2 Pure Fe with KCl sample exposed to the environment simulation for 24 h.

The following figure shows the results of the pure Fe with KCl sample exposure to 20 % water vapor, 5 % O_2 and 75 % N_2 environment at 400 °C for 24 h.

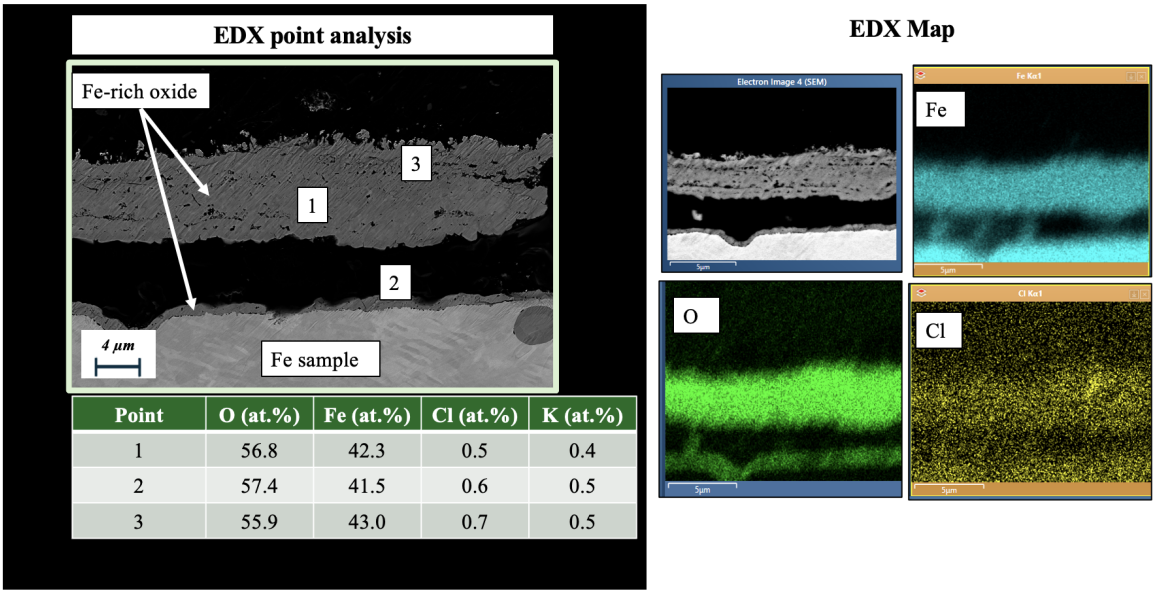

Point	O (at.%)	Fe (at.%)	Cl (at.%)	K (at.%)
1	56.8	42.3	0.5	0.4
2	57.4	41.5	0.6	0.5
3	55.9	43.0	0.7	0.5

Figure 4.3: shows the SEM-EDX figure of Fe with KCl sample exposed for 24 h. The at.% in the table stands for atomic percent.

4.3.3 Pure Fe with KCl sample exposed to the environment simulation for 168 h.

The following figure shows the results of the pure Fe with KCl sample exposure to 20 % water vapor, 5 % O_2 and 75 % N_2 environment at 400 °C for 168 h.

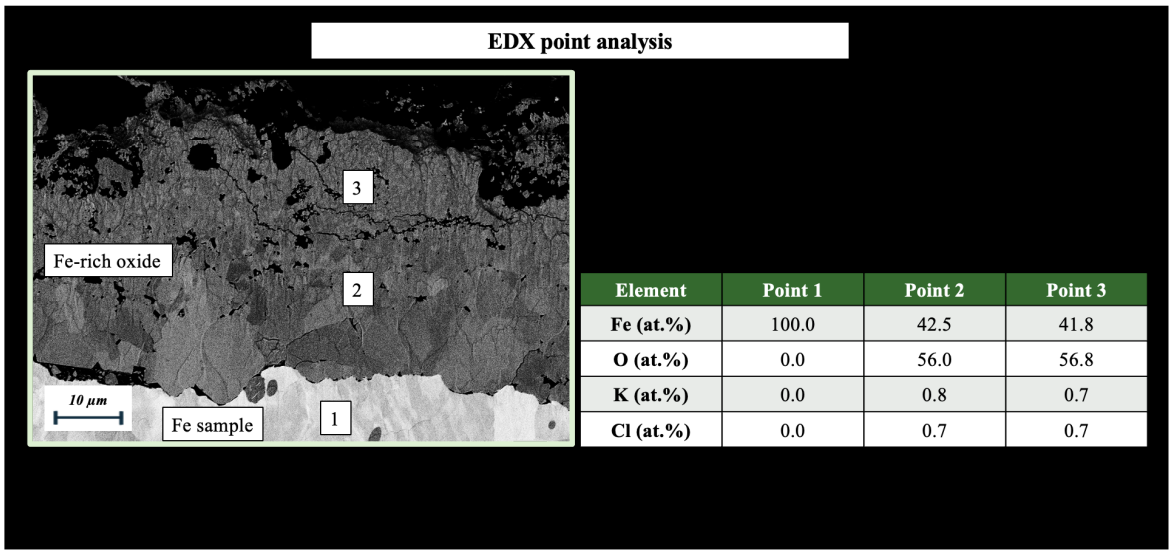

Element	Point 1	Point 2	Point 3
Fe (at.%)	100.0	42.5	41.8
O (at.%)	0.0	56.0	56.8
K (at.%)	0.0	0.8	0.7
Cl (at.%)	0.0	0.7	0.7

Figure 4.4: shows the SEM-EDX figure of Fe with KCl sample exposed for 168 h. The at.% in the table stands for atomic percent.

4.4 Imaging results from SEM

The SEM figures below show the results of the simulated environment of the superheater tubes. These allow the analysis of the oxide scale thickness and identification of oxide grain presence in the oxide scale on the sample post exposure to simulation. The raw version of the SEM figures can be found in appendix A.

4.4.1 Pure Fe samples exposed to environment simulation for 24 h

The following figure shows the results of pure Fe sample exposure to 20 % water vapor, 5 % O_2 and 75 % N_2 environment at 400 °C for 24 h. There were no oxide grains identified, and the oxide scale thickness was approximately 3.5 μm.

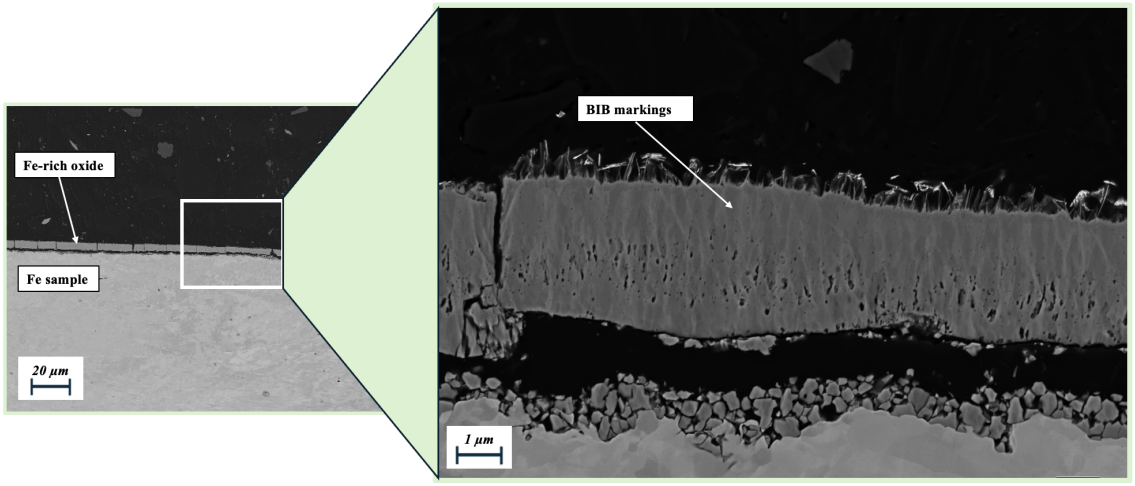

Figure 4.5: shows the figure from the SEM analysis of the sample of pure Fe exposed to 20 % water vapor, 5 % O_2 and 75 % N_2 environment at 400 °C for 24 h. The SEM is at magnification of 1000 and 1800.

4.4.2 Pure Fe samples exposed to environment simulation for 168 h

The following figure shows the results of exposure of pure Fe sample to 20 % water vapor, 5 % O_2 and 75 % N_2 environment at 400 °C for 168 h. In the figure, oxide grains were identified and the longest had an approximate length of 1.8 μm. The length of the oxide scale was also approximately 10 μm.

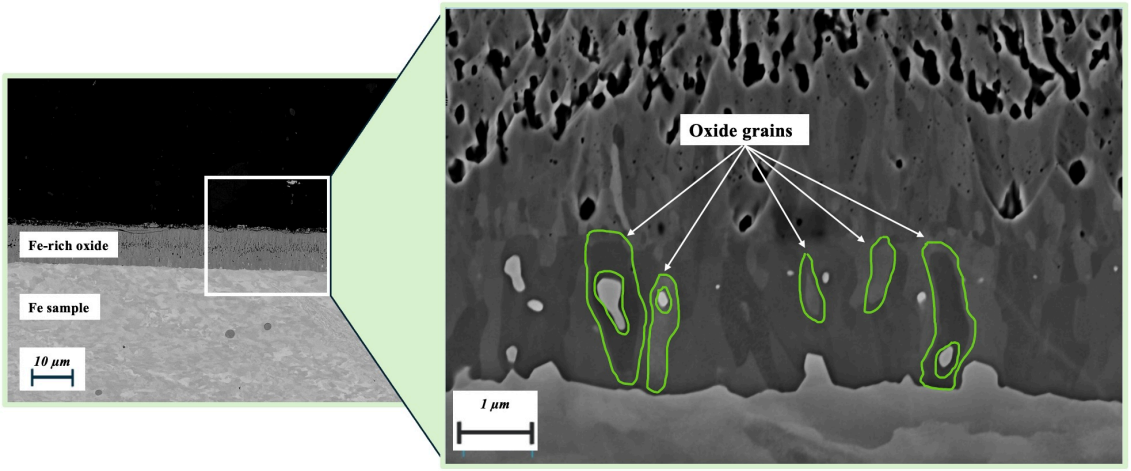

Figure 4.6: shows the figure from the SEM analysis of the sample of pure Fe exposed to 20 % water vapor, 5 % O_2 and 75 % N_2 environment at 400 °C for 168 h. The SEM is at magnification of 1000 and 12000.

4.4.3 Pure Fe with KCl samples exposed to the environment simulation for 24 h.

The following figure shows the results of pure Fe with KCl sample exposure to 20 % water vapor, 5 % O_2 and 75 % N_2 environment at 400 °C for 24 h. In the figure, oxide grains were identified and the longer had an approximate length of 0.5 μm. The oxide scale length was also approximately 9.8 μm.

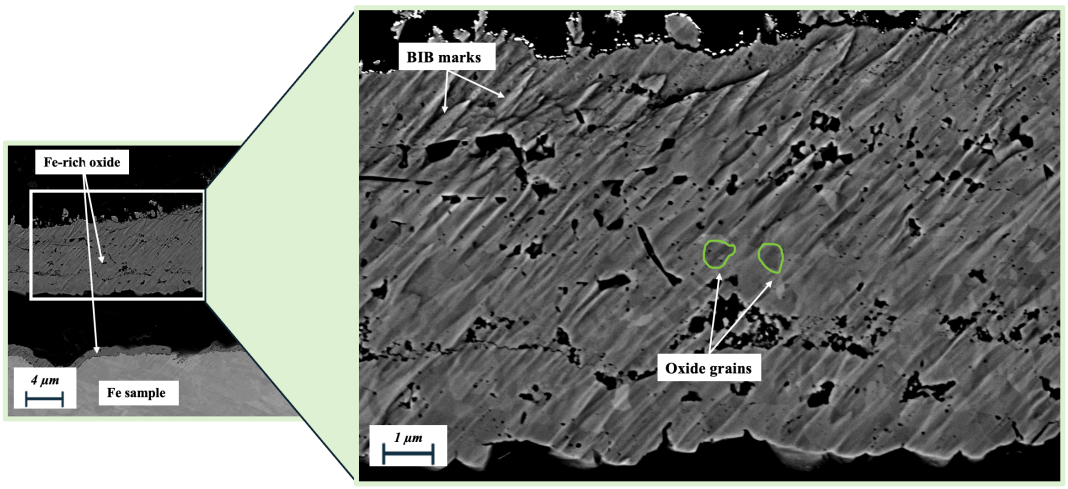

Figure 4.7: shows the figure from the SEM analysis of the sample of pure Fe exposed to 20 % water vapor, 5 % O_2 and 75 % N_2 environment at 400 °C for 24 h. The SEM is at magnification of 6300 and 20000.

4.4.4 Pure Fe with KCl samples exposed to the environment simulation for 168 h.

The following figure shows the results of pure Fe with KCl sample exposure to 20 % water vapor, 5 % O_2 and 75 % N_2 environment at 400 °C for 168 h. In the figure, oxide grains were identified and the longest had an approximate length of 8.0 μm. The oxide scale length was also approximately 37 μm.

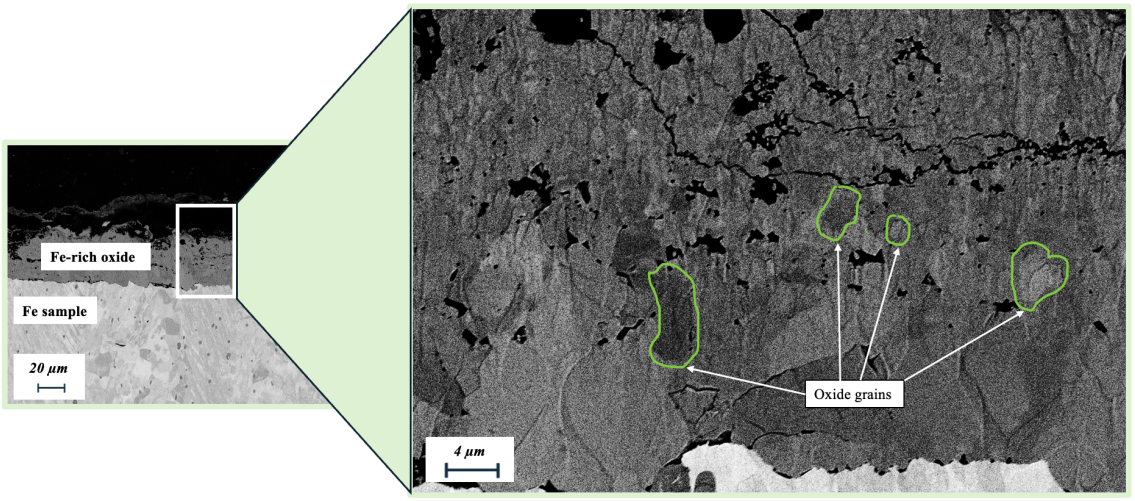

Figure 4.8: shows the figure from the SEM analysis of the sample of pure Fe exposed to 20 % water vapor, 5 % O_2 and 75 % N_2 environment at 400 °C for 168 h. The SEM is at magnification of 1000 and 5580.

4.5 BIB milling method

Since the samples were planned to be analyzed cross-sectionally, the improvement of the mechanical polishing on the samples' surface was performed by implementing the flat BIB-milling technology. Below are the SEM figures that were taken to perform comparison before and after BIB milling.

4.5.1 Post and Pre BIB milling of pure Fe samples exposed for 24 h

The following figure shows the results of pure Fe sample exposure to 20 % water vapor, 5 % O_2 and 75 % N_2 environment at 400 °C for 24 h.

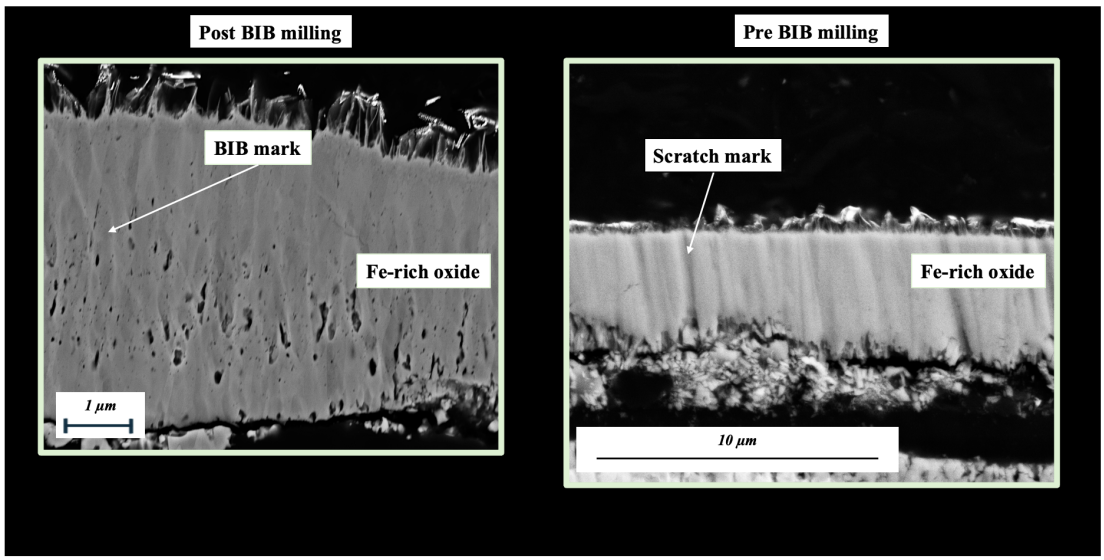

Figure 4.9: shows the figure from the SEM analysis of the sample of pure Fe exposed to 20 % water vapor, 5 % O_2 and 75 % N_2 environment at 400 °C for 24 h. The SEM is at magnification of 20000 and 15000.

4.5.2 Post and Pre BIB milling of pure Fe samples exposed for 168 h

The following figure shows the results of pure Fe sample exposure to 20 % water vapor, 5 % O_2 and 75 % N_2 environment at 400 °C for 168 h.

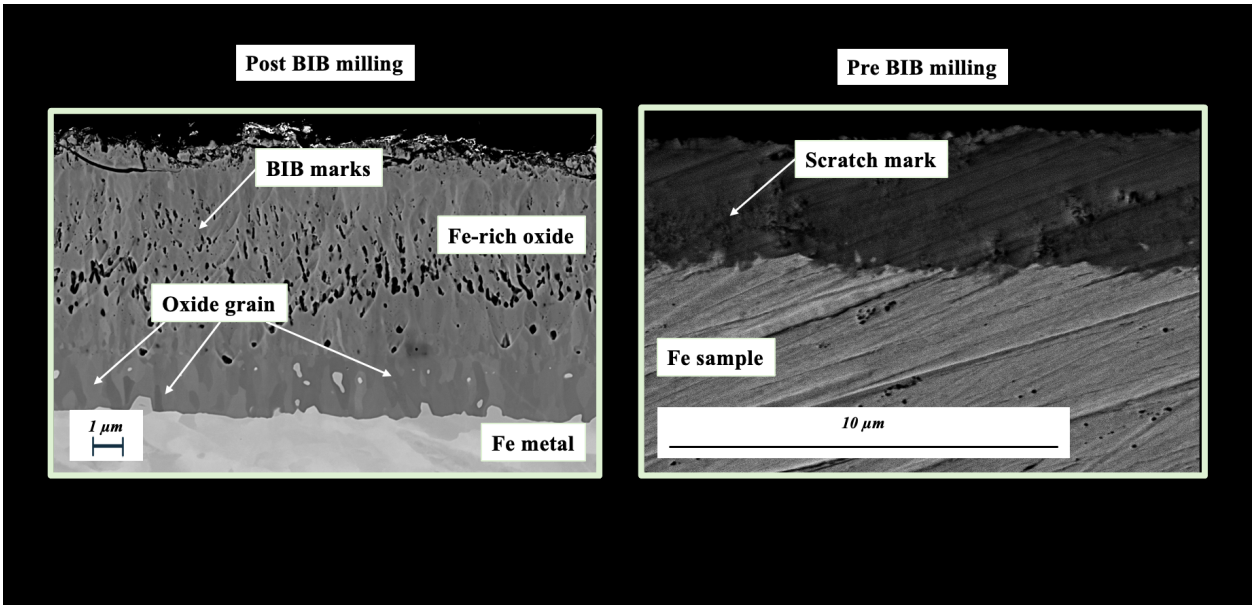

Figure 4.10: shows the figure from the SEM analysis of the sample of pure Fe exposed to 20 % water vapor, 5 % O_2 and 75 % N_2 environment at 400 °C for 168 h. The SEM is at magnification of 6300 and 8883.

4.5.3 Post and Pre BIB milling of pure Fe with KCl samples exposed for 24 h

The following figure shows the results of pure Fe with KCl sample exposure to 20 % water vapor, 5 % O_2 and 75 % N_2 environment at 400 °C for 24 h.

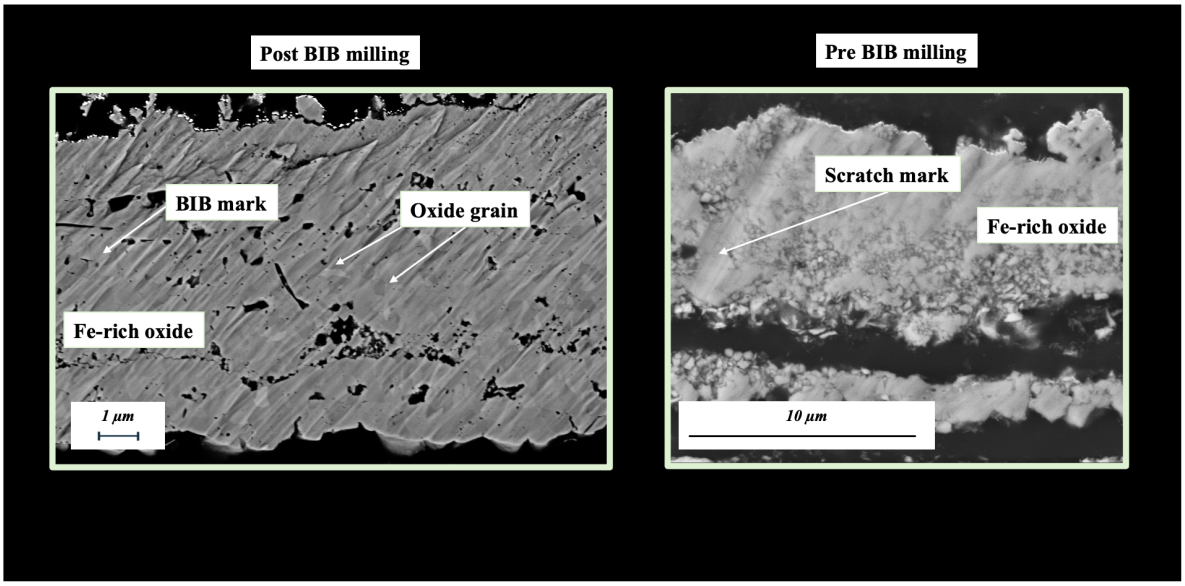

Figure 4.11: shows the figure from the SEM analysis of the sample of pure Fe exposed to 20 % water vapor, 5 % O_2 and 75 % N_2 environment at 400 °C for 24 h. The SEM is at magnification of 6300 and 13086.

5
Discussion

In order to provide an answer to this study which aims to investigate the microstructure of oxide scales formed in environments relevant to biomass- and waste-fired boilers, the acquired figures from SEM and gravimetric analysis will be utilized. This study also aimed to evaluate how KCl may affect both the corrosion kinetics and oxide grain in the oxide scale on the pure Fe surface. To simulate the high-temperature environment of the superheater tubes in the boiler, the furnace was given an environment where the air flow had 20 % water vapor, 5 % O_2 and 75 % N_2 environment at 400 °C at either 24 h or 168 h of sample exposure.

As figure 4.1 illustrates, the gravimetric analysis for pure Fe samples exposed to 20 % water vapor, 5 % O_2 and 75 % N_2 at 400 °C showed that there was a mass gain for both pure Fe samples and Fe with KCl samples that were exposed in the furnace for 24 h and 168 h. This shows that the oxide scale on the pure Fe samples that were exposed for longer period of time experienced greater oxide scale growth, which corroborates the earlier literature [15]. In table 4.1, Fe samples that were exposed for 168 hours showed almost twice the mass gain of the samples exposed for 24 h. Similar results were demonstrated by pure Fe with KCl samples as the 168 h of exposure to the simulated environment has caused its mass gain to be more than three times larger than the mass gain of Fe with KCl samples that were exposed for 24 h. This demonstrates that both exposure time and presence of KCl have positive effect on corrosion process.

The standard deviation in the data sets for the two exposure time and group of samples are presented in figure 4.1. For the pure Fe samples that were exposed for 24 h and 168 h, the standard deviations are smaller, which show that there is a small amount of mass variation between the samples that were exposed. However, the standard deviations are higher for pure Fe with KCl samples that were exposed for 24 h or 168 h. In addition, pure Fe with KCl samples showed the highest standard deviation value. These results imply that the samples had a higher mass variation after their respective exposure to the simulated environment. As mentioned in section 2.2.4, previous literature has shown that Fe-based alloys such as FeCrMo were more susceptible to detachment of oxide scale when KCl is present in the environment which causes reoccurrence of corrosion on the sample's surface. Although the samples used in this study were pure Fe, this earlier finding may explain the higher mass variation for pure Fe with KCl samples that were exposed for 168 h.

For Au samples that were exposed for an hour, the gravimetric result presented in

table 4.2 shows that there is a small decrease in the mass of the Au samples after the exposure. The cause of the samples' mass decrease is difficult to establish as this could be either caused by the sublimation of KCl from the Au samples or that the KCl on the samples had fallen during their placement and extraction from the furnace. To further evaluate if the presence of alumina crucible with KCl in the furnace can prevent KCl sublimation, the exposure can be run for a longer time.

With the help of SEM, it was possible to obtain figures of the cross-sectional area of Fe samples that were exposed to the simulated environment. The figures of pure Fe samples that were exposed for 24 h as presented in figure 4.5 show that were no oxide grains in the oxide scale, and the oxide scale thickness was approximately 3.5 μm. The figures of pure Fe samples that were exposed for 168 h as presented in figure 4.6 show that oxide grains were identified and the longest had an approximate length of 1.8 μm. The oxide scale length was also approximately 10 μm. The figures of pure Fe with KCl samples that were exposed for 24 h as presented in figure 4.7 show that oxide grains were identified and the longer oxide grain had an approximate length of 0.5 μm. The oxide scale length was also approximately 9.8 μm. The figures of pure Fe with KCl samples that were exposed for 168 h as presented in figure 4.7 show that oxide grains were identified and the longest had an approximate length of 8.0 μm. The oxide scale length was also approximately 37 μm. These results shows that the pure Fe samples that were exposed longer to the simulated environment experienced corrosion process to a higher extent due to the resulting thicker oxide scale on the Fe sample surface. In addition, the presence of KCl appears to have increased the rate of corrosion due to the thicker oxide scale lengths, higher mass gain of the samples, and that oxide grains were detected for both exposure times.

The utilization of the SEM-EDS (EDX) figures enabled both EDX mapping and EDX point analysis of the exposed samples. The results of these are presented in figure 4.2, figure 4.3, and figure 4.4. This made the identification of the Fe sample surface, and the Fe-rich oxide scales as well as the layer of the KCl on the Fe-rich oxide scales possible. In figure 4.3 for example, it was possible to identify that there was a detachment between the Fe-rich oxide scale and the Fe sample surface. The EDX point analysis for samples with KCl as presented in figure 4.3 and figure 4.4, showed that there is a small amount left of the KCl on the sample surface post exposure. This could be due to the preparation process before SEM that caused the dissolution of KCl.

To evaluate the flat BIB milling technology implemented on the sample preparation, figure 4.9, figure 4.10 and figure 4.11 were presented. These figures made it possible for the identification and differentiation of oxide grain, flat BIB milling marks, and scratch marks from mechanical polishing, and this can be clearly identified in figure 4.10 for the Fe sample exposed for 168 h. On the other hand, figure 4.11 illustrates that it can be difficult to differentiate oxide grains from the flat BIB milling marks. This shows that improvement with the flat BIB milling technique is needed, which can be conducted by testing the variation in the accelerated voltage, the angle of incident of the ion beam and the exposure time of the flat BIB milling.

6
Conclusion

In conclusion, the flat BIB milling method, when combined with SEM, has the potential to reveal oxide grains at the nanoscale, making the observation of these oxide grains in the oxide scale more accessible than with widely utilized conventional technologies and techniques. Nevertheless, this study also shows that the method requires further development. Therefore, future work should focus on optimizing the BIB parameters to achieve the best possible Fe surface finish. Lastly, exposure time and the presence of KCl appear to have a positive effect on the detection of oxide grains and the growth of the oxide scale on pure Fe samples.

Bibliography

[1] NBC news. First climate migrants arrive in Australia from sinking Tuvalu in South Pacific [Internet]. USA: NBC; 2025 [2025 dec 12; 2026 feb 8]. Available from: https://www.nbcnews.com/world/asia/first-climate-migrants-arrive-australia-sinking-tuvalu-south-pacific-rcna248792

[2] Australian Government: Department of Foreign Affairs. Australia-Tuvalu Falepili Union treaty [Internet]. Australia;2026 [2026 mars 30]. Available from https://www.dfat.gov.au/geo/tuvalu/australia-tuvalu-falepili-union-treaty

[3] Lindmark, H. High-Temperature Corrosion in Biomass- and Waste-fired Boilers: Current Challenges and the Impact of Integrating Carbon Capture Technology. Gothenburg, Sweden: Chalmers University of Technology; 2025. Available from: https://research.chalmers.se/en/publication/546647

[4] United Nations. Atmosphere [Internet]. USA. United Nations [2026 feb 8]. Available from: https://sdgs.un.org/topics/atmosphere

[5] Abas N, Kalair A, Khan N. Review of fossil fuels and future energy technologies. Science Direct. 2015; 69(1): pages 31-49. DOI:https://doi.org/10.1016/j.futures.2015.03.003

[6] Gryparis E, Rzeszutko M, Papadopulos P, Manousakis N, Psomopoulos CS. Correlation analysis of population, energy consumption and overshoot day global trends. Discover Sustainability. 2025; 6(1):pages 1-16. Available from: https://doi.org/10.1007/s43621-025-02088-7

[7] Malinauskaite J, Jouhara H, Czajczyńska D, Stanchev P, Katsou E, Rostkowski P, et al. Municipal solid waste management and waste-to-energy in the context of a circular economy and energy recycling in Europe. Energy. 2017: pages 2013-2044. DOI: https://doi.org/10.1016/j.energy.2017.11.128

[8] Ericsson K, Werner S. The introduction and expansion of biomass use in

Swedish district heating systems. Biomass and Bioenergy. 2016;94(1):pages 57-65. DOI: https://doi.org/10.1016/j.biombioe.2016.08.011

[9] Phother-Simon J, Hanif I, Liske J. Jonsson T. The influence of a KCl-rich environment on the corrosion attack of 304 L:3D FIB/SEM and TEM investigations. Corrosion Science. 2021; 183(1). DOI: https://doi.org/10.1016/j.corsci.2021.109315

[10] The International Energy Agency (IEA). Energy System of Sweden [Internet]. France: IEA; 2026 [2026 feb 10]. Available from: https://www.iea.org/countries/sweden

[11] IRENA – International Renewable Energy Agency. Power to heat and cooling: Status [Internet]. Abu Dhabi: IRENA; 2025 [2025 nov 25]. Available from:https://www.irena.org/Innovation-landscape-for-smart-electrification/Power-to-heat-and-cooling/Status#:~:text=Status%20and%20pace%20of%20progress,2035%20(IPCC%2C%202018)

[12] Johansson LG, Svensson JE, Skog E, Pettersson J, Pettersson C, Folkeson N, Asteman H, Jonsson T, Halvarsson M. Critical corrosion phenomena on superheaters in biomass and waste-fired boilers. J. Iron Steel Res. Int. 2007;14(5):pages 35-39. DOI:https://doi.org/10.1016/S1006-706X(08)60048-5

[13] Ekroth I, Granryd E. Tillämpad termodynamik.1:5. Lund: Studentlitteratur AB; 2006.

[14] Pedefferi P. Corrosion Science and Engineering [Internet]. Milan, Italy: Springer, Cham; 2018. [2026 mars 6]. DOI: https://link.springer.com/chapter/10.1007/978-3-319-97625-9_26

[15] Pujilaksono B, Jonsson T, Halvarsson M, Svensson JE, Johansson LG. Oxidation of iron at 400-600°C in dry and wet O_2. Corrosion Science. 2010; 52: sidor 1560-1569. DOI: https://doi.org/10.1016/j.corsci.2010.01.002

[16] Lienig J. Electromigration and its impact on physical design in future technologies. ACM International Symposium on Physical Design (ISPD). 2013: pages 33-34. DOI:10.1145/2451916.2451925.

[17] Sabioni ACS, Souza JN, Ji V, Jomard F, Trindade VB, Carneiro JF. Study of ion diffusion in oxidation films grown on a model Fe–15 % Cr alloy. Solid State Ionics. 2015;276:1-8. DOI: https://doi.org/10.1016/j.ssi.2015.03.027

[18] Persdotter A. Beyond Breakaway Corrosion: Investigating the Secondary corrosion protection of Iron-based alloys [Internet]. Gothenburg, Sweden: Chalmers University of Technology; 2023. [2026 mars 23]. Available from: https://research.chalmers.se/publication/537954

[19] Hanke, L.D., Schenk, K.H., Scholz, D.R. Broad Beam Ion Milling for Microstructure Characterization. MPC. 2016; 5(5):pages 767-779. DOI: http://dx.doi.org/10.1520/MPC20160049.

[20] Society for Mining Metallurgy & Exploration Inc. 361.2.4 Scanning Electron Microscope Analysis (SEM). In: XXXI IMPC-International Mineral Processing Congress [Internet]. Society for Mining, Metallurgy, and Exploration (SME); 2024 [2026 Feb 7]. Available from: https://research.ebsco.com/linkprocessor/plink?id=f5f6f44f-44ee-3e0f-8b86-c0d91f688b3a

[21] Fan W, Hamilton A, Patel JP, Salmond JA, Gualtieri AF. Determining factors affecting the accuracy of SEM-EDX data-based quantitative chemical analysis for identifying naturally occurring individual carcinogenic erionite fibers. Scientific Reports. 2025;15(1). DOI:10.1038/s41598-025-09551-5

[22] Rise Research Institutes of Sweden (RISE). SEM with EDX/EDS [Internet]. Sweden. RISE [2026 Feb 8]. Available from: https://www.ri.se/en/metrology/service/scanning-electron-microscopy-sem-with-energy-dispersive-x-ray-analysis-edx-eds

A

Appendix 1: Raw Data

The following are the obtained SEM figures of the samples that were exposed to the environment simulation.

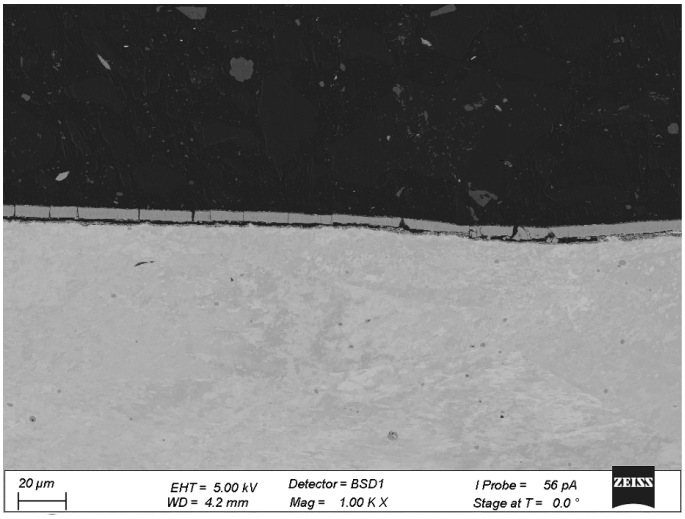

Figure A.1: shows the raw SEM figure of pure Fe samples exposed to 20 % vapor, 5 % O_2 and 75 % N_2 environment at 400 °C for 24 h.

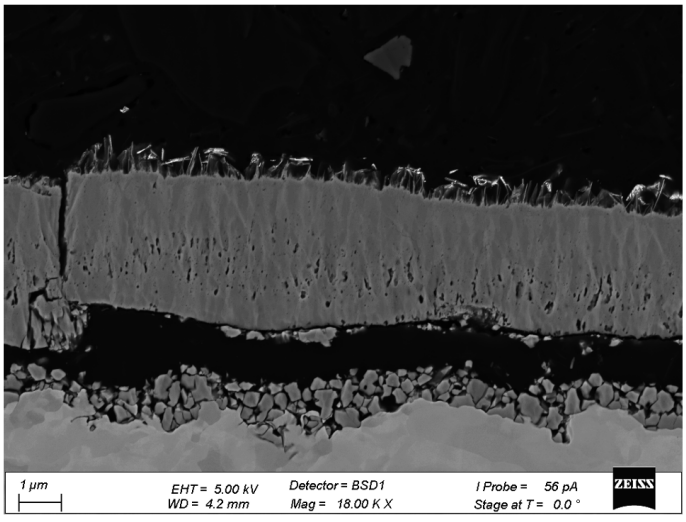

Figure A.2: shows the raw SEM figure of pure Fe samples exposed to 20 % vapor, 5 % O_2 and 75 % N_2 environment at 400 °C for 24 h.

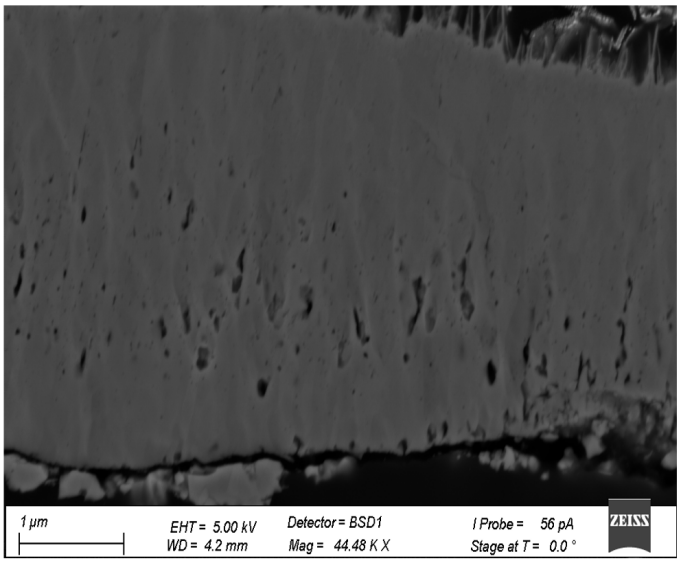

Figure A.3: shows the raw SEM figure of pure Fe samples exposed to 20 % vapor, 5 % O_2 and 75 % N_2 environment at 400 °C for 24 h.

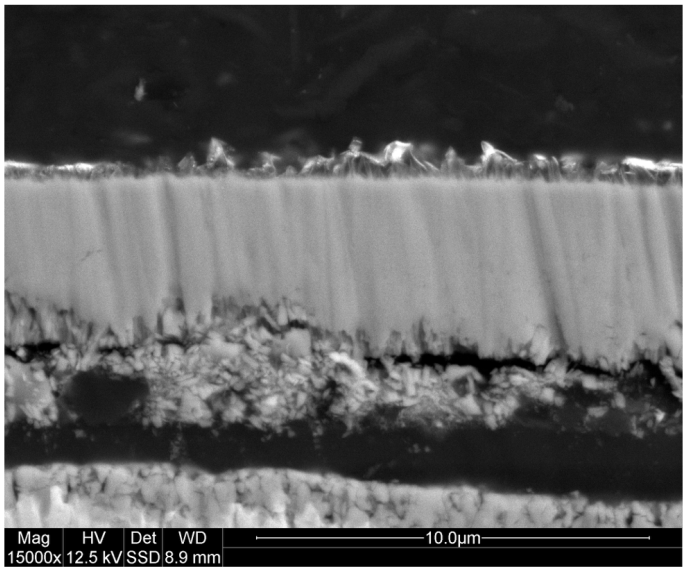

Figure A.4: shows the raw SEM figure of pure Fe samples exposed to 20 % vapor, 5 % O_2 and 75 % N_2 environment at 400 °C for 24 h.

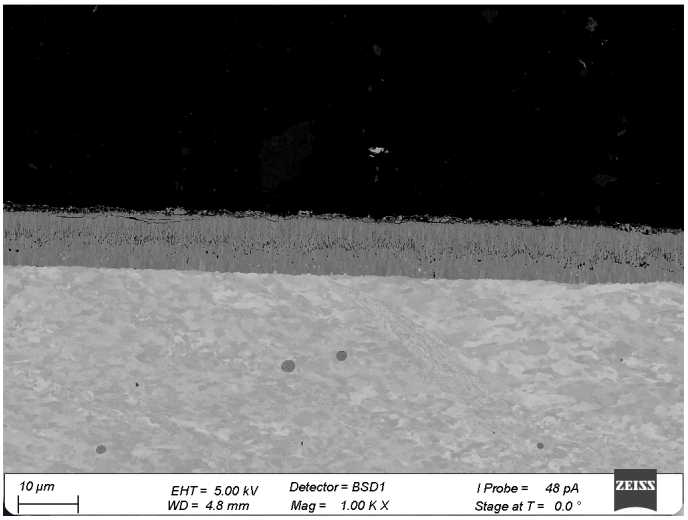

Figure A.5: shows the raw SEM figure of pure Fe samples exposed to 20 % vapor, 5 % O_2 and 75 % N_2 environment at 400 °C for 168 h.

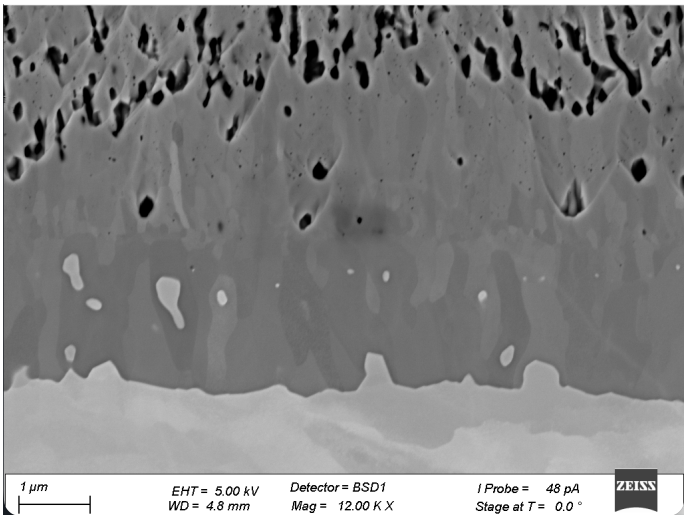

Figure A.6: shows the raw SEM figure of pure Fe samples exposed to 20 % vapor, 5 % O_2 and 75 % N_2 environment at 400 °C for 168 h.

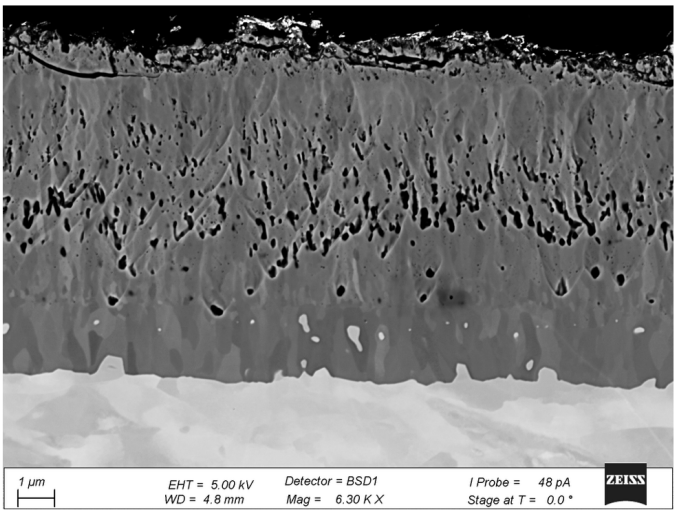

Figure A.7: shows the raw SEM figure of pure Fe samples exposed to 20 % vapor, 5 % O_2 and 75 % N_2 environment at 400 °C for 168 h.

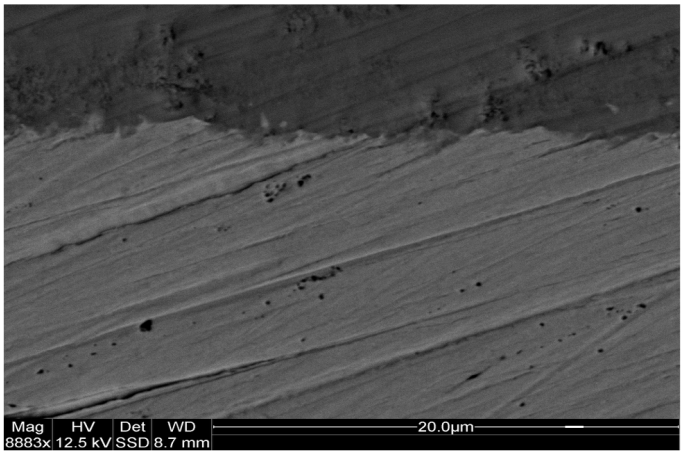

Figure A.8: shows the raw SEM figure of pure Fe samples exposed to 20 % vapor, 5 % O_2 and 75 % N_2 environment at 400 °C for 168 h.

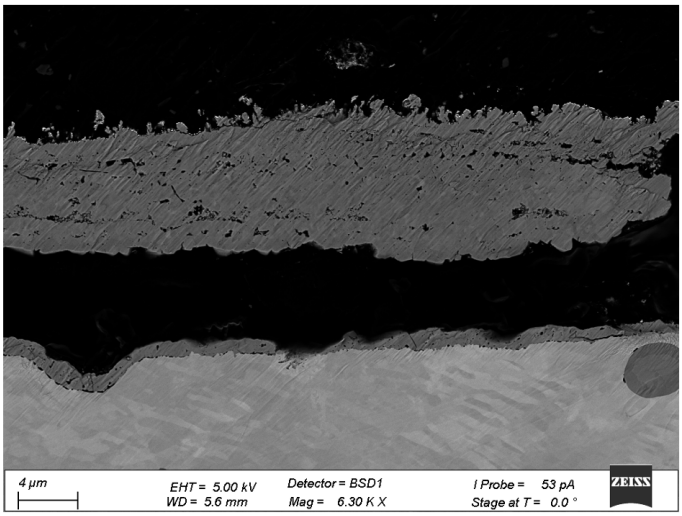

Figure A.9: shows the raw SEM figure of pure Fe with KCl samples exposed to 20 % vapor, 5 % O_2 and 75 % N_2 environment at 400 °C for 24 h.

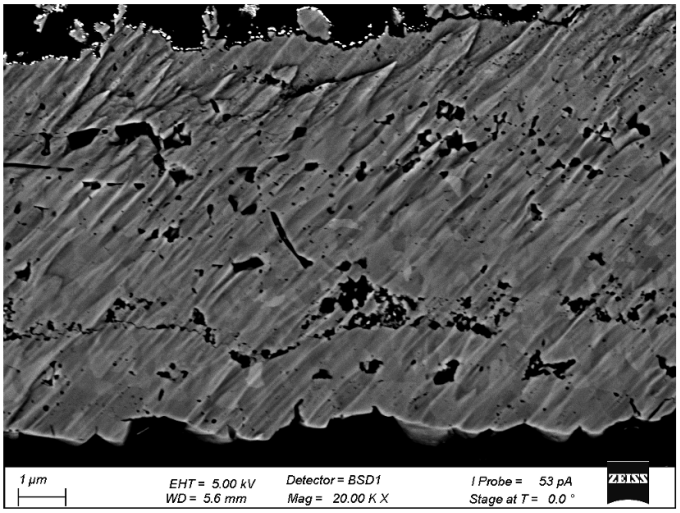

Figure A.10: shows the raw SEM figure of pure Fe with KCl samples exposed to 20 % vapor, 5 % O_2 and 75 % N_2 environment at 400 °C for 24 h.

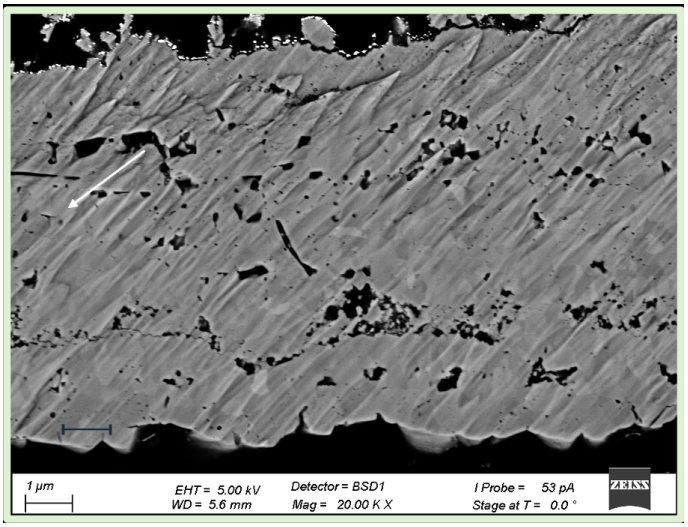

Figure A.11: shows the raw SEM figure of pure Fe with KCl samples exposed to 20 % vapor, 5 % O_2 and 75 % N_2 environment at 400 °C for 24 h.

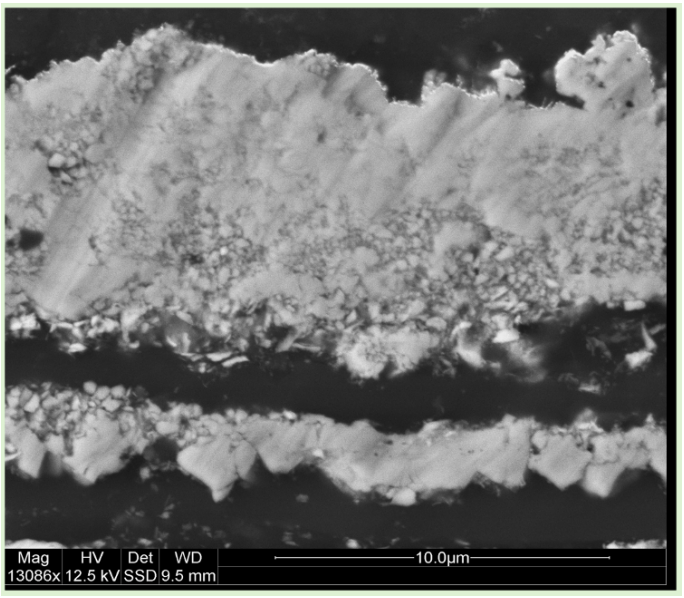

Figure A.12: shows the raw SEM figure of pure Fe with KCl samples exposed to 20 % vapor, 5 % O_2 and 75 % N_2 environment at 400 °C for 24 h.

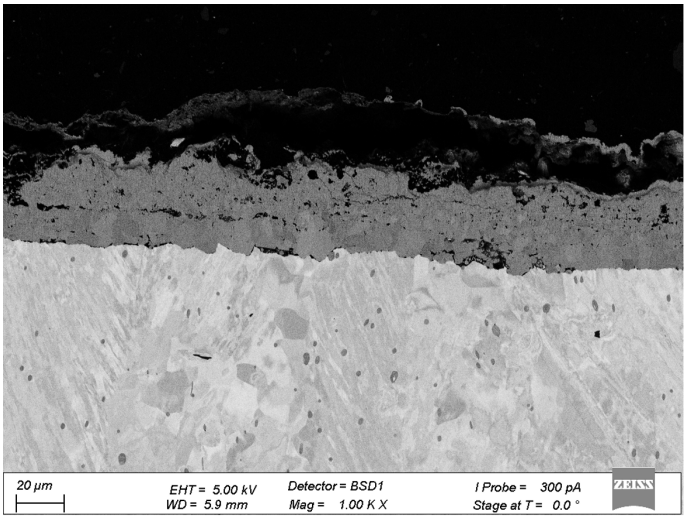

Figure A.13: shows the raw SEM figure of pure Fe with KCl samples exposed to 20 % vapor, 5 % O_2 and 75 % N_2 environment at 400 °C for 168 h.

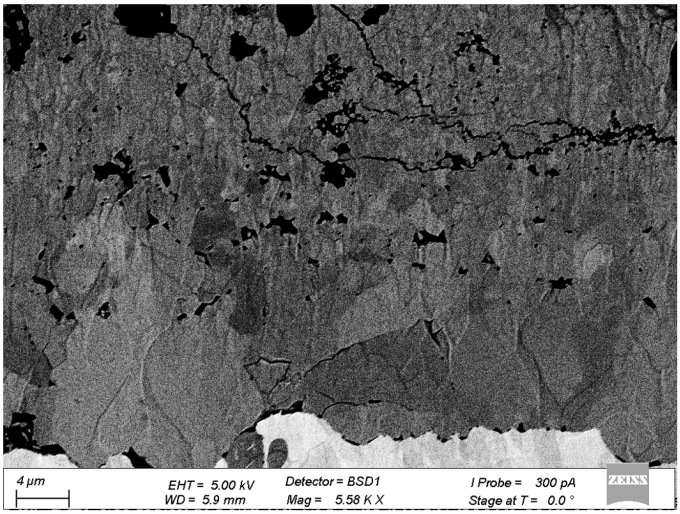

Figure A.14: shows the raw SEM figure of pure Fe with KCl samples exposed to 20 % vapor, 5 % O_2 and 75 % N_2 environment at 400 °C for 168 h.

Division of Energy and Materials, Department of Chemistry and Chemical Engineering
CHALMERS UNIVERSITY OF TECHNOLOGY
Gothenburg, Sweden
www.chalmers.se